Mon. Not. R. Astron. Soc. **371,** 583–608 (2006) doi:10.1111/j.1365-2966.2006.10722.x

Stellar populations in bulges of spiral galaxies*

Bhasker K. Moorthy† and Jon A. Holtzman

Department of Astronomy, New Mexico State University, PO Box 30001, MSC 4500, Las Cruces, New Mexico 88003, USA

Accepted 2006 June 19. Received 2006 June 19; in original form 2005 December 12

ABSTRACT

We present line strengths in the bulges and inner discs of 38 galaxies in the local Universe, including several galaxies whose bulges were previously identified as being disc like in their colours or kinematics, to see if their spectral properties reveal evidence for secular evolution. We find that red bulges of all Hubble types are similar to luminous ellipticals in their central stellar populations. They have large luminosity-weighted ages, metallicities, and α/Fe ratios. Blue bulges can be separated into a metal-poor class that is restricted to late types with small velocity dispersion and a young, metal-rich class that includes all Hubble types and velocity dispersions. Luminosity-weighted metallicities and α/Fe ratios are sensitive to central velocity dispersion and maximum disc rotational velocity. Red bulges and ellipticals follow the same scaling relations. We see differences in some scaling relations between blue and red bulges and between bulges of barred and unbarred galaxies. Most bulges have decreasing metallicity with increasing radius; galaxies with larger central metallicities have steeper gradients. Where positive age gradients (with the central regions being younger) are present, they are invariably in barred galaxies. The metallicities of bulges are correlated with those of their discs. While this and the differences between barred and unbarred galaxies suggest that secular evolution cannot be ignored, our results are generally consistent with the hypothesis that mergers have been the dominant mechanism responsible for bulge formation.

Key words: galaxies: bulges – galaxies: elliptical and lenticular, cD – galaxies: evolution – galaxies: formation – galaxies: spiral – galaxies: stellar content.

1 INTRODUCTION

Bulges are important relics of the galaxy formation process. An analysis of their structure, kinematics, dynamics, and stellar content can potentially reveal the physical mechanisms responsible for the formation and evolution of galaxies, as well as the nature of the Hubble sequence. Similarities between bulges and ellipticals have long been recognized but recent observations suggest that at least some bulges may be related to discs. This has led to the suggestion that the large bulges of early-type spirals are more similar to ellipticals, while late-type bulges are more disc like (Wyse, Gilmore & Franx 1997). As a consequence of these observations, formation scenarios have emerged for bulges that are either identical to those for ellipticals or involve the secular evolution of discs. However, the degree to which formation mechanisms are homogeneous is still open to question.

Early models for elliptical formation involved the monolithic collapse of a primordial gas cloud (Larson 1974; Carlberg 1984; Arimoto & Yoshii 1987). This model naturally explains several observed properties of ellipticals, including the mass–metallicity relation and the presence of metallicity gradients, but large-scale collapse is inconsistent with present-day cold dark matter (CDM) cosmology and with recent observations showing that massive ellipticals were not fully assembled until after $z = 1$ (Bell et al. 2004; Faber et al. 2005). It is now widely believed that ellipticals formed hierarchically through mergers of smaller fragments (Kauffmann, White & Guiderdoni 1993). Mergers are frequently caught in the act (van Dokkum et al. 1999; Ferreiro & Pastoriza 2004), and photometric and kinematic evidence for past mergers is abundant in ellipticals (Emsellem et al. 2004; van Dokkum 2005). The merger model has been extended to bulges due to the many observed similarities between bulges and ellipticals. For example, Carollo et al. (1997) found that bulges were well fitted by the $R^{1/4}$ law used for ellipticals. The Fundamental Plane relation of bulges is nearly the same as that of ellipticals, with late types perhaps lying below early types (Falcón-Barroso, Peletier & Balcells 2002).

In the secular evolution scenario, bulges are produced through radial and vertical transport of disc material as the result of instabilities and resonances (see Kormendy & Kennicutt 2004, for a review). These models come in several flavours, most of which involve bars. Simulations that do not include gas have found that

*Based on observations obtained with the Apache Point Observatory 3.5-m telescope, which is owned and operated by the Astrophysical Research Consortium.

†E-mail: bmoorthy@nmsu.edu

bars can buckle, heating the inner disc and increasing its scaleheight to resemble a bulge. Hydrodynamical simulations have found that bars can transport gas towards the centre, triggering intense star formation (Pfenniger 1993; Friedli & Benz 1995; Norman, Sellwood & Hasan 1996; Noguchi 2000; Immeli et al. 2004). The presence of neighbours may also drive this (Kannappan, Jansen & Barton 2004). Support for secular evolution comes from observed correlations between the scalelengths of bulges and their discs (Courteau, de Jong & Broeils 1996; MacArthur, Courteau & Holtzman 2003). It has also been found that the light profiles of many bulges are closer to exponential than $R^{1/4}$ (Andredakis & Sanders 1994; de Jong 1996a; Balcells et al. 2003; MacArthur et al. 2003; de Jong et al. 2004). Furthermore, the ratio of rotational to random motions in bulges is often typical of discs (Kormendy & Illingworth 1982; Kormendy & Kennicutt 2004). Comparisons between the morphology and kinematics of observed galaxies with simulated ones have shown that boxy and peanut-shaped (b/p) bulges are bars viewed at high inclination (Bureau & Freeman 1999; Aronica et al. 2003; Chung & Bureau 2004; Athanassoula 2005). Athanassoula (2005) distinguished between b/p bulges, which are formed through the buckling of the bar, and what she called ‘discy bulges’, which are smaller cold components that formed out of the gas driven inwards by the bar.

Bulges that could have been formed through secular evolution are often referred to as ‘pseudobulges’ to distinguish them from the ‘classical’ bulges that may have formed through mergers. Since pseudobulge signatures are generally found in late-type spirals, Kormendy & Kennicutt (2004) suggested that early-type spirals (Sa, Sab, and some S0) contain classical bulges, while late-type spirals (Sb, Sc and some S0) contain pseudobulges. On the theoretical side, Pfenniger (1993) found that secular evolution can produce small bulges but not those having a characteristic radius much larger than the disc scalelength. However, it is not at all clear that the spectrum of observed bulge properties points towards two distinct formation scenarios. Since the stability of bars continues to be debated (Debattista et al. 2004; Shen & Sellwood 2004; Bournaud, Combes & Semelin 2005), it is also not clear whether or not pseudobulges should exist only in present-day barred galaxies.

Stellar population (SP) studies can potentially place important constraints on the formation mechanisms. A succesful formation scenario has to reproduce the observed distribution of ages and metallicities. In a collapse model, bulges and ellipticals are universally old and have radial metallicity gradients. In his dissipative collapse simulation, Carlberg (1984) found that the steepness of the metallicity gradient was correlated with galaxy properties, such as mass and luminosity. If ellipticals and bulges formed through mergers, it is important to keep in mind that their assembly histories might be very different from their star formation histories. ΛCDM simulations suggest that most-massive ellipticals (and therefore presumably bulges) were not fully assembled until recently ($z < 1$), whereas the bulk of star formation occurred much earlier ($z > 2$) in the progenitor galaxies (De Lucia et al. 2006). This is consistent with observational studies of merger activity, number counts, and the luminosity function (Faber et al. 2005; van Dokkum 2005). De Lucia et al. found that the star formation histories of massive ellipticals peak at $z \sim 5$, while those of less-massive ellipticals peak at progressively smaller redshifts and are more extended. These simulations predict a mass–metallicity relation, with the most-massive ellipticals having solar metallicity and the least-massive ones being a factor of 10 smaller in metallicity. Gradients in SPs are difficult to model within the framework of hierarchical formation. Mergers between discs can presumably preserve existing gradients in the subcomponents and produce new gradients through gas infall, but mixing from successive mergers might erase any correlations between gradients and global properties. White (1980) found that the metallicity gradient in a disc galaxy was halved after three mergers with similar-sized discs. However, Bekki & Shioya (1999) found that more-massive galaxies had steeper metallicity gradients. The impact of secular evolution on gradients is not straightforward. Since the resulting pseudobulge has a smaller scalelength than the progenitor disc, an existing disc gradient could become amplified (A Klypin, private communication). However, mixing during secular evolution can have the effect of washing out existing gradients. Adding gas only complicates the picture. If gas is fuelled towards the central regions by bars, this could result in a nucleus that is younger and more metal rich than the outer regions of the bulge. Simulations by Friedli, Benz & Kennicutt (1994) resulted in a flattening of metallicity gradients in all but the innermost regions where a starburst, fuelled by infalling gas, produced a metal-rich nucleus.

Abundance ratios can place additional constraints. Mg and other α-elements are primarily produced in Type II supernovae (SNe II), while a substantial fraction of the Fe-peak elements, Fe and Cr, are produced in Type Ia supernovae (SNe Ia). Therefore, α-enhancement is generally attributed to a cessation of star formation before the bulk of SNe Ia occurred. Through chemical evolution modelling, Thomas (1999) found that a clumpy collapse model produced uniform α-enhancement or positive gradients (increasing α/Fe with radius), while a merger model produced uniformly solar α/Fe or negative gradients. For the case of secular evolution, Immeli et al. (2004) made different predictions for abundance ratios in bulge stars, depending on whether it is the gas disc or the stellar disc which first becomes unstable. In the former case, gas clumps merge together and spiral inwards, causing massive starbursts and producing large α/Fe ratios. In the latter case, a bar forms and then channels gas towards the centre. This occurs on long time-scales, resulting in smaller α/Fe ratios.

The only bulges where individual stars can be resolved are those of the Milky Way (MW) and M31. The majority of the stars in the MW bulge are old ($t \geqslant 7$ Gyr), although young ($t \leqslant 200$ Myr) and intermediate-age (200 Myr $\leqslant t \leqslant$ 7 Gyr) stars are also detected (Ibata & Gilmore 1995; Sadler, Rich & Terndrup 1996; Feltzing & Gilmore 2000; van Loon et al. 2003; Zoccali et al. 2003). As a barred late-type spiral, the MW might be a good candidate for secular evolution. However, the MW bulge is dominated by old stars unlike the MW disc at the solar neighbourhood. If the bulge was produced through a rearrangement of disc stars, either this must have occurred several Gyr ago or the inner disc must have a considerably different age distribution than the disc at the solar neighbourhood. The young stars in the bulge are mainly found in the innermost regions. While the gas that formed them could have been driven by a bar, it could just as well have been provided by a recent merger. The mean metallicity of the Galactic bulge is slightly subsolar (Minniti 1996; Feltzing & Gilmore 2000; van Loon et al. 2003; Zoccali et al. 2003; Fulbright, McWilliam & Rich 2006). The stellar content of M31’s bulge is not as well understood as that of the MW since we cannot reach its main-sequence turn-off. Observations of giant stars are consistent with M31’s bulge being similar in age to the MW bulge and slightly more metal rich (Rich 1999; Jablonka et al. 2000; Davidge 2001; Stephens et al. 2003; Sarajedini & Jablonka 2005).

SPs in more distant bulges have to be studied through photometry or spectroscopy of integrated light. An important limitation of such studies is that integrated light is dominated by the most-luminous stars. Colours have been studied more extensively as they have the advantage of higher signal-to-noise ratio (S/N). Pioneering work by Balcells & Peletier (1994) found that colour variations from galaxy to galaxy are much larger than colour differences between disc and bulge in each galaxy. Similarly, de Jong (1996b) found that bulge and disc colours are correlated and that the colour differences between bulge and disc suggested that the SPs did not vary much from one to the other. Unfortunately, colour studies suffer from degeneracies between ages, metallicities, and extinction.

Line strengths are nearly insensitive to dust (MacArthur 2005), provide information on the abundances of several elements and molecules, and allow for breaking the age–metallicity degeneracy. Worthey (1994) obtained line strengths for a range of single-age, single-metallicity SPs (SSPs) on the Lick/IDS system (Burstein et al. 1984; Faber et al. 1985) and found that while individual indices are sensitive to both age and metallicity, the relative sensitivity varies from index to index. Spectral indices have also been defined at high resolution (Vazdekis 1999), allowing better age determinations than otherwise possible. One of the limitations of the original models is that they were calibrated using galactic stars that do not cover an adequate range of metallicity and α/Fe ratio for interpreting the spectra of early-type galaxies (they contain very few, if any, stars that are both metal rich and α-enhanced). Much progress has since been made in extending Lick indices to non-solar abundance ratios using synthetic spectra or by calibrating with globular clusters that, like early-type galaxies, are both metal rich and α-enhanced (Tripicco & Bell 1995; Trager et al. 2000a; Thomas, Maraston & Bender 2003; Thomas, Maraston & Korn 2004; Lee & Worthey 2005).

Line strengths have been used extensively to characterize the SPs of ellipticals. The luminosity-weighted ages of massive ellipticals are large ($\sim$10 Gyr) while those of low-mass ellipticals ($\sigma \lesssim 130$ km s^{-1}) are, on average, smaller ($\sim$5 Gyr), with a large spread (Caldwell, Rose & Concannon 2003; Nelan et al. 2005; Thomas et al. 2005). Ellipticals in low-density environments appear to show larger scatter in their SPs than those in clusters (Rose et al. 1994; Trager et al. 2000a; Vazdekis et al. 2001; Proctor & Sansom 2002; Denicoló et al. 2005; Thomas et al. 2005). These observations go against the collapse model and confirm, at least qualitatively, the prediction of the merger model by Kauffmann (1996). Mg-sensitive indices in ellipticals are more tightly correlated with central velocity dispersion than Fe-sensitive indices, resulting in a correlation between Mg/Fe and σ_0 (Bender, Burstein & Faber 1993). Worthey & Collobert (2003) found that the Mg–σ relation of ellipticals is consistent with these objects having been formed through around 50 mergers with merger probability constant or mildly declining with time.

There have been fewer studies of line strengths in bulges. Integrated light studies on the bulges of the MW and M31 have arrived at similar ages and metallicities as the resolved studies (Puzia et al. 2002; Puzia, Perrett & Bridges 2005). Both bulges have large SSP ages. M31 is slightly supersolar in SSP metallicity, while the MW is solar. Both are α-enhanced with M31 being more so in line with its larger σ_0. Early studies on extragalactic bulges found them to be similar to ellipticals in their central line strengths (Idiart, de Freitas Pacheco & Costa 1996; Jablonka, Martin & Arimoto 1996). Proctor & Sansom (2002) found that bulges have smaller average luminosity-weighted age than ellipticals. These authors did not find the correlation predicted by Kauffman (1996) for bulges and suggested that it might have been erased by secular evolution in late types. The largest sample of bulges to date was that of Prugniel, Maubon & Simien (2001), who identified three classes of bulges: (i) young bulges which are small, have ionized gas, low velocity dispersions, and low metallicity; (ii) old bulges that are α-enhanced and follow the mass–metallicity relation of ellipticals; and (iii) bulges that have a mixture of young and old populations, which are less α-enhanced than those of class (ii), and deviate from the Mg_2 relation of ellipticals. Prugniel et al. and Proctor et al. found that both Fe and Mg were correlated with σ_0 in bulges, resulting in the lack of a tight correlation between Mg/Fe and σ_0 in bulges. Prugniel et al. (2001) found that Mg_2 in bulges is more tightly correlated with the $V_{\rm max}$ of the disc than with σ, indicating that the SPs are more sensitive to the total galaxy potential (i.e. the dark matter halo) than the bulge potential.

Studies with spatial resolution offer several advantages over studies that only sample the central region. First, differential studies of ages and abundances are more reliable than absolute estimates. Secondly, formation models invariably make predictions for the global properties of galaxies which are better traced by mean observed quantities than central ones; observations with spatial resolution allow estimation of mean values. Finally, as mentioned already, population gradients can place additional constraints on formation mechanisms.

Line-strength gradients have been studied extensively in ellipticals. Carollo, Danziger & Buson (1993) and Forbes, Sánchez-Blázquez & Proctor (2005) found strong correlations between gradients and physical properties, while others found weak (Mehlert et al. 2003) or no (Kobayashi & Arimoto 1999) correlations. There have been relatively few studies on gradients in bulges. Fisher, Franx & Illingworth (1996) found steeper metallicity gradients along the minor-axes of nine edge-on S0s than along the major-axes, suggesting different formation mechanisms for the bulge and the disc. Goudfrooij, Gorgas & Jablonka (1999) found that gradients were correlated with luminosity in 16 bulges. Proctor, Sansom & Reid (2000) found that gradients correlated with velocity dispersion, albeit with a sample of only four galaxies, while Jablonka, Gorgas & Goudfrooij (2002) found no such correlation. Integral field spectroscopy has enabled the acquisition of 2D line strengths in bulges with results just starting to emerge (e.g. Sil'chenko et al. 2003; Falcón-Barroso et al. 2004). Recent work by Ryder, Fenner & Gibson (2005) showed that tunable filters might be another way to obtain 2D line strengths.

In this paper, we present line strengths and line-strength gradients in the bulges and inner discs of 38 galaxies. Our sample, described in Section 2, was chosen to span a range of bulge properties and specifically targetted several galaxies with blue bulges and similar bulge/disc colours and/or disc-like kinematics in an attempt to look for SP signatures of secular evolution. Section 3 describes the observations and data analysis. Section 4 describes the SP results and Section 5 discusses their implications for bulge formation scenarios. Section 6 contains a summary. The structure, kinematics, and dynamics and how they relate to the SPs will be discussed in a future paper (hereafter Paper II).

2 THE GALAXY SAMPLE

We selected a sample that included some bulges that are similar in colour to their discs and others that are considerably redder as a control. Colour was chosen as the primary selection criterion because this has so far been the best-studied property of bulges. de Jong (1996b, hereafter DJ) and Peletier & Balcells (1997, hereafter PB) obtained colour gradients of galaxies from the Uppsala General Catalog (Nilson 1973) with major-axes larger than 2 arcmin. We selected 17 galaxies from PB and 14 from DJ. The two samples complement each other nicely in their sky coverage and sampling of Hubble types. The DJ galaxies are nearly face-on while the PB galaxies are highly inclined.

We also included three galaxies, NGCs 2787, 3384 and 3945, which were previously found to possess disc-like structural and kinematical properties (Busarello et al. 1996; Erwin et al. 2003; Pinkney et al. 2003; Sil'chenko et al. 2003). All three are barred S0 galaxies with inner discs or bars that are more luminous than the surrounding bulge. One of the PB galaxies, NGC 7457, is also known to have disc-like kinematics (Kormendy 1993; Pinkney et al. 2003). Michard & Marchal (1994) found small bar-like distortions in this galaxy and Emsellem et al. (2004) found nearly-cylindrical rotation which is seen in boxy bulges (Bertola & Capaccioli 1977; Kormendy & Illingworth 1982; Falcón-Barroso et al. 2004) and in simulations of edge-on bars (Combes et al. 1990; Sellwood 1993; Athanassoula & Misiriotis 2002).

This project initially began in collaboration with some members of the ENEAR survey (Wegner et al. 2000). Therefore, the first five galaxies we observed were from their sample: NGCs 4472, 2775, 3544, 3831 and 5793. NGC 4472, a bright elliptical in the centre of the Virgo cluster, was included for comparison with previous studies. The other four galaxies were selected to span a wide range in inclination and bulge-to-disc ratio.

Several reasons for including both high- and low-inclination galaxies are listed below.

(1) Minor-axis observations of highly inclined galaxies offer minimum disc contamination in the outer regions of the bulge.

(2) In moderately inclined galaxies, there is actually more disc contamination along the minor-axis than the major-axis for the same solid angle. To estimate the degree of disc contamination, we obtained spectra along both major- and minor-axes for some of our inclined galaxies.

(3) Major-axis observations of inclined galaxies allow for the measurement of rotation which can provide additional information about the structure of the galaxy.

(4) Low-inclination galaxies have less disc contamination in the central regions and allow for clear identification of bars, rings, and other morphological features. Including both high- and low-inclination galaxies allows for a comparison between bars and b/p bulges.

(5) In highly inclined galaxies, the bulge and disc can be distinguished based on their shapes (spheroidal versus flat). In face-on galaxies, this is not possible and so bulges are generally defined as the excess light on top of the inward extrapolation of an exponential disc. SPs and kinematics offer two additional and independent means of distinguishing between bulges and discs in face-on galaxies.

12 out of our 20 low-inclination galaxies are barred. Some of our highly inclined galaxies were classified by Lütticke, Dettmar & Pohlen (2000) into peanut-shaped, boxy, nearly boxy, or elliptical bulges. For our remaining highly inclined galaxies, we determined the shapes using their technique. This yielded 10 b/p bulges and eight elliptical bulges. Therefore, the fraction of barred galaxies in low-inclination galaxies is approximately equal to the fraction of b/p bulges in highly inclined galaxies. While peanut-shaped bulges are easily identified, it is not always easy to distinguish an elliptical bulge from one that is slightly boxy. For instance, Lütticke et al. classified NGC 5838's bulge as elliptical but Michard & Marchal (1994) described it as boxy.

Table 1 contains basic data on our galaxies. The column 'Morphological type' describes the shape of the bulge if the galaxy is highly inclined (boxy, peanut, or elliptical) and whether or not it is barred if it is not highly inclined. Identifications marked with an asterisk are those of Lütticke et al., while those without asterisks are our identifications.

When comparing SPs in galaxies with different colours, it is important to keep in mind that colour is correlated with the global dynamical properties of a galaxy. Fig. 1 shows the bulge $B - K$ colours as a function of central velocity dispersions, and maximum disc rotational velocities of our galaxies where available. The bulge and disc colours are from DJ and PB. Bulge colour is defined to be the colour at half the K-band bulge effective radius or 5 arcsec, whichever is larger. Disc colour is defined to be the colour at two disc scalelengths. We found that it is useful to subdivide bulges according to whether they are redder or bluer than $B - K = 4$; these are shown as red and blue points. Section 3.3 describes how the rotation curves and velocity dispersion profiles were obtained. Central velocity dispersion was measured on approximately 4-arcsec spectral bins [3.3, 4.2 and 3.8 arcsec for Double Imaging Spectrograph (DIS) I, II and III, respectively]. The maximum disc rotational velocity shown is the average of visual estimates on either side of the major-axis. In this and subsequent plots, the point shape represents the Hubble type; the circles are S0 galaxies; the hexagons are S0a and Sa galaxies; the pentagons are Sab galaxies; the squares are Sb galaxies; and the triangles are Sbc and Sc galaxies. The filled symbols are barred galaxies. The thin open symbols are elliptical bulges if highly inclined and unbarred galaxies if not highly inclined. The thick open symbols are b/p bulges.

Bulge colours correlate more tightly with $V_{\max}$ than with σ_0. Galaxies with $V_{\max} > 200$ km s^{-1} host red bulges while those with $V_{\max} < 165$ km s^{-1} host blue bulges. Both red and blue bulges are found in nearly the full range of central velocity dispersions spanned by our galaxies although there is an overabundance of red bulges in large σ galaxies and vice versa.

3 OBSERVATIONS AND DATA ANALYSIS

3.1 Observations

Observations were made with the DIS on the ARC 3.5-m telescope at Apache Point Observatory between 2000 January and 2004 February. The spectrograph uses a dichroic to split the light into separate blue and red channels. During this period, the instrument was upgraded in several phases with the installation of new detectors and optics. Table 2 gives the specifications of each configuration and Table 3 describes the spectroscopic observations. DIS I gave us continuous wavelength coverage from 4000 to 7500 Å while DIS II and DIS III gave us continuous coverage from 3700 to 7500 Å. A 5 arcmin × 1.5 arcsec slit was used in all the observations. On each night, we observed a quartz lamp for flat-fielding, arc lamps for wavelength calibration, and two to five spectrophotometric standards for flux calibration. On several nights, Lick standard stars from Worthey et al. (1994) were observed to allow us to transform our line indices to the Lick/IDS system.

For most of the highly inclined galaxies, we obtained spectra along both major- and minor-axes. For the unbarred low-inclination galaxies, we obtained major-axis profiles except for NGC 2916 for which we obtained a minor-axis profile instead because there was a bright star along the major-axis. For the clearly barred galaxies, we placed the slit along the bar. For IC 302 and NGC 2487, this is different from the position angle of the major-axis. In NGC 5375, the bar happens to be along the major-axis. We could not identify a major-axis in NGC 266 or NGC 5020, but the slit must have been

Table 1. The galaxy sample. DJ denotes de Jong (1996b), PB denotes Peletier & Balcells (1997), and EN denotes the ENEAR survey (Wegner et al. 2000). The morphological types are from the NED. The *B* magnitudes are from RC3 (de Vaucouleurs et al. 1991). The bulge and disc colours are from DJ and PB. Bulge colour is defined to be the colour at half the *K*-band bulge effective radius or 5 arcsec, whichever is larger. Disc colour is defined to be the colour at two disc scalelengths. b/a is the red major- over minor-axis ratio taken from the sources listed. The recessional velocities shown are the RC3 heliocentric velocities corrected to the Local Group according to Karachentsev & Makarov (1996). The 21-cm values were used where both 21-cm and optical velocities were available. Since no RC3 data were available for NGC 3831, the *B* magnitude and optical heliocentric velocity were taken from Fairall et al. (1992). The scale was obtained assuming $H_0 = 70$. The distance to NGC 3384 was determined by Cepheid observations (Tanvir, Ferguson & Shanks 1999).

Galaxy	Source	Type	Morphological type	m_B (mag)	$(B-K)_B$	$(B-K)_D$	b/a	V_{LG} (km s^{-1})	Scale (kpc arcsec^{-1})
IC 267	DJ	SBb	Unbarred	13.63	4.6	4.24	0.71	3577	0.25
IC 302	DJ	SBbc	Barred	13.59			0.92	5950	0.41
IC 1029	PB	SAb	Elliptical*	13.64	3.89	3.77	0.24	2520	0.17
NGC 266	DJ	SBab	Barred	12.33	4.6	3.85	0.94	4908	0.34
NGC 765	DJ	SABbc	Barred	13.60	4.4	3.82	1.00	5117	0.37
NGC 1642	DJ	SA(rs)c	Unbarred?	13.28	4.0	3.26	1.00	4579	0.32
NGC 2487	DJ	SBb	Barred	13.10	4.1	3.53	0.92	4758	0.33
NGC 2599	DJ	SAa	Unbarred	13.12	4.0	3.8	1.00	4651	0.32
NGC 2775	EN	SAab	Unbarred	11.13			0.85	1173	0.08
NGC 2787		SB0+	Barred	11.77				696	0.06
NGC 2916	DJ	SAab	Unbarred	12.42	4.2	3.59	0.74	3618	0.25
NGC 3384		SB0-	Barred	10.63				735	0.06
NGC 3544	EN	SABa	Unbarred?	12.99			0.30	3354	0.23
NGC 3681	DJ	SAB(r)bc	Barred	12.25	3.8	3.47	1.00	1239	0.08
NGC 3728	DJ	SAb	Unbarred	13.80	4.2	3.7	0.75	6904	0.48
NGC 3831	EN	SAB0+	Boxy*	14.5			0.24	4715	0.33
NGC 3883	DJ	SAb	Barred	13.10	4.1	3.44	0.91	6937	0.48
NGC 3945		SB0+	Barred	11.38				1220	0.09
NGC 4472	EN	E2		9.30				744	0.05
NGC 5020	DJ	SABbc	Barred	12.50	3.6	3.11	0.85	3284	0.23
NGC 5326	PB	SAa	Unbarred	12.92	4.05	3.97	0.50	2573	0.18
NGC 5362	PB	SAb	Unbarred	13.14	3.56	3.24	0.37	2314	0.16
NGC 5375	DJ	SBab	Barred	12.40	3.9	3.47	0.81	2418	0.17
NGC 5389	PB	SABO/a	Boxy*	13.10	4.12	4.10	0.20	1996	0.14
NGC 5422	PB	SA0	Elliptical*	12.81	4.17	4.09	0.20	1921	0.13
NGC 5577	PB	SAbc	Elliptical*	13.05	3.84	3.54	0.28	1702	0.12
NGC 5689	PB	SBO/a	Boxy?*	12.54	4.14	4.12	0.25	2295	0.16
NGC 5707	PB	SAab	Elliptical*	13.38	4.24	3.92	0.25	2354	0.16
NGC 5719	PB	SABab	Boxy?*	13.1	4.54	3.84	0.36	1676	0.12
NGC 5746	PB	SABb	Peanut*	11.38	4.42	4.50	0.16	1676	0.12
NGC 5793	EN	SABb	Boxy?	14.30			0.37	3387	0.23
NGC 5838	PB	SA0-	Boxy?*	11.74	4.21	4.11	0.35	1338	0.09
NGC 5987	PB	SAb	Elliptical	13.00	4.46	4.14	0.40	3207	0.22
NGC 6246A	DJ	SABc	Unbarred	14.10	3.9	3.23	0.91	5495	0.38
NGC 6368	PB	SAb	Elliptical*	13.10	4.84	4.58	0.20	2904	0.20
NGC 7311	PB	SAab	Elliptical	13.36	4.35	4.07	0.50	4762	0.33
NGC 7332	PB	SAB0	Boxy*	12.11	3.75	3.58	0.26	1584	0.11
NGC 7457	PB	SAB0-	Boxy?	11.86	3.69	3.50	0.52	1115	0.08
NGC 7537	PB	SAbc	Elliptical*	13.65	3.88	3.62	0.34	2888	0.20

placed close to it as we see substantial rotation. We did not detect any rotation in five galaxies: IC 302 and NGCs 765, 2487, 2916 and 6246A, due to their inclinations being too low.

We obtained images in *B*, *V* and *R* for bulge-to-disc decomposition (B/D) on six nights using the SPIcam detector on the same telescope. Typical exposure times were 600 s for *B*, 180 s for *V*, and 120 s for *R*. Superbiases and twilight flats were obtained on each night.

3.2 Basic reductions

Data reduction was carried out using the XVISTA software package. For the imaging, basic reduction included bias subtraction and flat-fielding. For the spectroscopy, flat-fields were constructed using a median of five to 10 bright quartz lamp exposures; the mean spectral response was divided out. Wavelength calibration was performed using He, Ne, and Ar arc lamp exposures, using a fifth-order polynomial for both blue and red channels. Flux calibration was performed using a spline fit to published spectra of the spectrophotometric standards (Massey et al. 1988). Line curvature along the slit was measured using the lamp exposures and a simple row-by-row shift was stored for subsequent corrections. Similarly, spatial distortion in the spectrograph was measured using standard star exposures and the correction was stored.

Since spatial distortion includes a component due to differential refraction unless the slit is perpendicular to the parallactic angle, this component was calculated and removed from the standard star measurements. Differential refraction causes a mixture of light loss and positional shift along the slit as a function of wavelength depending

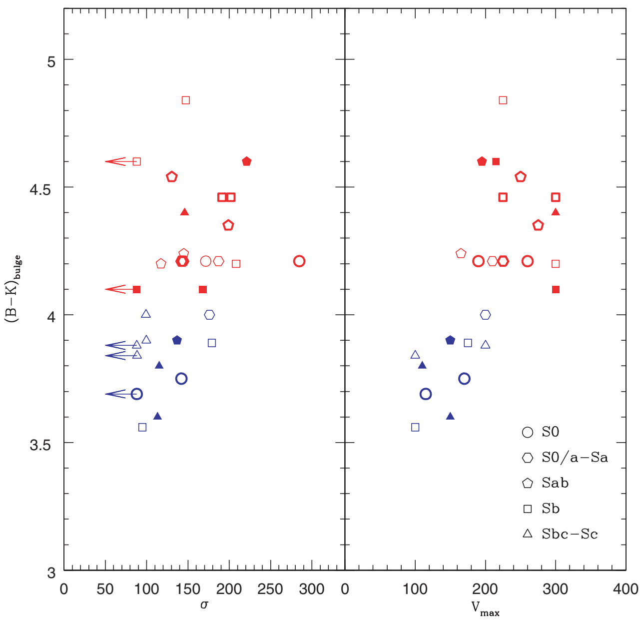

Figure 1. Bulge colour versus central velocity dispersion and maximum disc rotational velocity. The velocities are from this work while the colours are from PB and DJ. The central velocity dispersions were measured within an aperture of approximately 4 arcsec. See Table 1 for the definition of bulge colour. Bulges are shown in red or blue according to whether they are redder or bluer than $B - K = 4$. The filled symbols are barred galaxies. The thin open symbols are elliptical bulges if highly inclined and unbarred galaxies if not highly inclined; the thick open symbols are b/p bulges.

on the orientation of the slit to the parallactic angle. Light loss from differential refraction has a negligible effect on line strengths since they are defined over a relatively narrow range in wavelength. Positional changes as a function of wavelength need to be considered to ensure that the indices at different wavelengths are being compared at the same physical location. To do this, we calculate the expected shift from differential refraction depending on the orientation of the slit, assuming typical atmospheric parameters, and correct the position of the spectra as a function of wavelength accordingly. This is done for both flux calibration stars and the galaxy spectra; additionally, the corrected calibration stars provide a measurement of distortion that we also apply to the galaxies. An alternative, and perhaps more standard, approach would be to just ‘straighten’ each object based on the centroid or peak of the object. We felt that the calculated positional correction might be more accurate in the case of more diffuse galaxies, especially at wavelengths with lower S/N; in practice, they yield similar corrections.

Each galaxy frame was subtracted by the overscan and superbias, flat-fielded, and trimmed to remove the overscan region. The line curvature and spatial distortion corrections were applied. Multiple observations of each galaxy were then co-added, rejecting cosmic ray outliers in the process. Where multiple observations were not available, cosmic rays were removed by eye using a spatial median filter. Variance frames were propogated throughout the reduction process. To combine the red and blue channels, the red galaxy spectra were rescaled to spatially match the blue spectra. The spectra were then extracted in approximately 1-arcsec bins near the centre of the galaxy and using larger bins farther out. An average of sky values measured on both sides of the galaxy was subtracted from each slice. Wavelength and flux calibrations were applied and both red and blue frames were rebinned to 3 Å pixel^{-1}. Finally, the spectra were de-redshifted and the red and blue sides were combined. The blue spectrum was used out to a wavelength of 5600 Å and the red from 5450 Å. In the overlap region between 5450 and 5600 Å, an average of red and blue values was used. In some galaxies, there is a discontinuity in the overlap region that arises from the difficulty of accurately combining the two channels for extended objects; fortunately, none of our absorption features falls within this region.

On our last observing run (2004 February 15), the light on star frames was too extended to be explained by seeing alone. The excess light, which we believe is scattered light, had a spectral energy distribution similar to that of the mashed stellar spectrum but without any narrow spectral features presumably because it is significantly defocused. Since adding a constant to a spectrum decreases the equivalent width (EW) of an absorption feature and since the relative contribution of the scattered light to galaxy light increases with distance from the galaxy centre, this introduces an artificial negative gradient in the line-strength profiles. To correct for the scattered light, we fit the 2D stellar spectrum with a smoothed stellar spectrum along the wavelength direction and a fifth-order polynomial along the spatial direction, masking out the central 20 pixels (8.4 arcsec). This spatial profile, combined with the smoothed spectral profile of the galaxy, was subtracted from each galaxy frame. One galaxy that was observed on the problematic night, NGC 3384, has previously measured index profiles. Applying the correction resulted in much better agreement with the published values (see Section 3.7). No scattered light correction was applied on any of the other nights, since the correction derived for those nights did not affect the line-strength profiles significantly.

3.3 Measuring and correcting for rotation and velocity dispersion

We measured rotation and velocity dispersion in the stellar components of our galaxies using the PPXF package (Cappellari & Emsellem 2004). SSP spectra were constructed using the SP models by Bruzual & Charlot (2003, hereafter BC03) assuming a Chabrier initial mass function. The PPXF routine fits each galactic extraction with a linear combination of SSP spectra, shifting and broadening these to match the galaxy's rotation and velocity dispersion,

Table 2. Spectrograph specifications during our observing runs.

Detector	Observation dates (M/D/Y–M/D/Y)	Grating	Dispersion (Å pixel^{-1})	Approximate resolution (Å)	Scale (arcsec pixel^{-1})
DIS I blue	1/10/00–2/11/02	Medium	3.18	5.7	1.086
DIS I red	1/10/00–2/11/02	Medium	3.53	8.6	0.605
DIS II blue	4/13/02–10/09/02	Low	3.05	8.6	0.600
DIS II red	4/13/02–04/07/03	Medium	3.13	7.8	0.605
DIS III blue	03/06/03–02/15/04	Low	2.42	7.7	0.419
DIS III red	05/29/03–02/15/04	Medium	2.31	6.9	0.396

Table 3. Spectrographic observations.

Galaxy	Axis	Position angle	Date (M/D/Y)	Exposure time (s)
IC 267		−25	12/22/03	1 × 2400
				1 × 1230
IC 302	Bar	8	10/9/02	2 × 2400
IC 1029	Major	152	5/30/03	3 × 2400
NGC 266	Bar	0	9/17/02	2 × 2400
NGC 765		15	12/22/03	3 × 2400
NGC 1642		0	12/1/03	2 × 2400
NGC 2487	Bar	45	2/11/02	3 × 2400
NGC 2599		−90	2/11/02	3 × 2400
NGC 2775	Major	66	1/10/00	3 × 1200
	Minor	156	1/10/00	3 × 1200
NGC 2787	Major	109	2/15/04	2 × 2400
NGC 2916	Minor	−80	12/1/03	2 × 2400
				1 × 900
NGC 3384	Major	50	2/15/04	2 × 2400
NGC 3544	Major	−84	1/10/00	3 × 1200
	Minor	6	4/25/00	3 × 1200
NGC 3681	Bar	−25	2/11/02	3 × 2400
NGC 3728	Major	20	3/6/03	3 × 2400
NGC 3831	Major	24	4/25/00	3 × 1200
	Minor	114	5/3/00	3 × 1800
NGC 3883	Major	−14	3/7/03	3 × 2400
				1 × 1200
NGC 3945	Major	−22	2/15/04	2 × 2400
				1 × 1800
NGC 4472		67	1/10/00	3 × 1200
NGC 5020	Bar	38	3/6/03	2 × 2400
NGC 5326	Major	−44	5/4/00	4 × 1800
	Minor	−134	2/11/02	2 × 2400
NGC 5362	Major	−92	6/16/01	4 × 2400
NGC 5375	Bar	−10	4/7/03	1 × 2400
				1 × 1200
NGC 5389	Major	3	5/2/00	4 × 1800
	Minor	−87	5/2/00	3 × 1800
NGC 5422	Major	−26	5/2/00	2 × 1200
	Minor	64	5/3/00	2 × 1800
				2 × 1500
NGC 5577	Major	56	1/10/00	3 × 1200
				2 × 1500
NGC 5689	Major	−93	6/17/01	3 × 2400
	Minor	0	4/13/02	2 × 2400
NGC 5707	Major	39	5/29/03	2 × 2400
				1 × 1200
NGC 5719	Major	−90	5/30/03	3 × 2400
NGC 5746	Major	−9	4/17/02	3 × 2400
	Minor	−99	4/17/02	3 × 2400
NGC 5793	Major	−35	5/4/00	1 × 1800
	Minor	55		2 × 1500
NGC 5838	Major	42	6/8/02	2 × 2400
NGC 5987	Major	−109	5/30/03	1 × 2400
				1 × 2700
NGC 6246A		−90	2/19/01	2 × 1800
			2/20/01	2 × 1800
NGC 6368	Major	47	6/29/03	1 × 2400
				1 × 2100
NGC 7311	Major	24	7/1/03	1 × 2400
		15	10/12/01	1 × 2400
NGC 7332	Major	−24	7/3/00	4 × 1800
NGC 7457	Major	−38	7/1/03	1 × 2400
				1 × 1257
NGC 7537	Major	−100	10/12/01	4 × 2400

respectively. The fit was performed within the wavelength range 4800–5400 Å, with the emission lines Hβ, [O III] 4959, and [O III] 5007 masked out. The profiles will be presented in Paper II.

The galaxy spectrum at each location was shifted by the measured stellar rotation before measuring the line indices. To correct the indices for velocity dispersion, line strengths were measured on an SSP template that was broadened by the measured velocity dispersion and another template that was broadened only to the instrumental resolution. These templates were also constructed using a linear combination of BC03 SSP spectra with emission lines masked out, but the wavelength range for the fit was 4000–6600 Å, to include all the Lick indices. The same templates were used for emission correction (following section). The measured absorption-line EWs were multiplied by the ratio of the unbroadened line strength to the broadened one; for magnitudes, the correction factor is the difference between these two quantities.

3.4 Measuring and correcting for emission

Some absorption indices can be severely affected by line-filling by emission. These include the Balmer indices, Fe5015 (due to [O III] 5007 emission), and Mgb (due to [N I] 5199 emission). To correct for this, we subtracted the template described in the previous section from each galaxy spectrum. If on the residual spectrum, Hα was found to be in emission at the 5σ level and a local maximum was detected at Hβ, a Gaussian was fitted to the Hβ emission and subtracted from the galaxy spectrum. This procedure was repeated for Hγ and Hδ. [O III] 5007 and [N I] 5199 were subtracted out if they were found to be in emission at the 3 and 4σ levels, respectively. A larger threshold was used for [N I] 5199 because this feature lies at the edge of the Mg_2 absorption feature and spurious discontinuities often show up there due to template mismatch.

EWs were measured for several emission lines to study the nature of the ionized gas in bulges and inner discs. The galaxy continuum, obtained by smoothing the galaxy spectrum, was added to the emission spectrum described above before measuring the EWs.

3.5 Lick index measurements

The final galaxy spectra were broadened to 9.5-Å full width at half-maximum (FWHM), which is approximately equal to the Lick resolution, and rebinned to a dispersion of 0.125 Å pixel^{-1}. Variable broadening as prescribed in Worthey & Ottaviani (1997) was tried and found not to produce significantly different results. The strengths of 25 absorption features were measured using the latest bandpasses from Guy Worthey's webpage. The EW or magnitude of each feature was computed following Trager et al. (1998).

Spectral indices were measured on Lick standard stars, exactly as done for the galaxies, to transform our line strengths to the Lick/IDS system. Such transformations are necessary because our detector differs in resolution from the IDS and because the IDS spectra were not flux calibrated. Twenty-four stars ranging in spectral type from F5V to K7III were used in deriving the transformations for DIS I and 22 stars (also ranging in spectral type from F5V to K7III) were used for DIS III. By imaging one of the stars at several positions along the slit, it was determined that the line strengths do not vary significantly with slit position. Fig. 2 compares the indices we obtained for the stars with those obtained using the IDS. Linear least-squares fits were performed on these data to obtain the transformation terms. The final EWs and magnitudes were computed as follows:

$$\mathrm{EW} = \frac{\mathrm{EW_{raw}}\,T_0/T + B}{A}$$

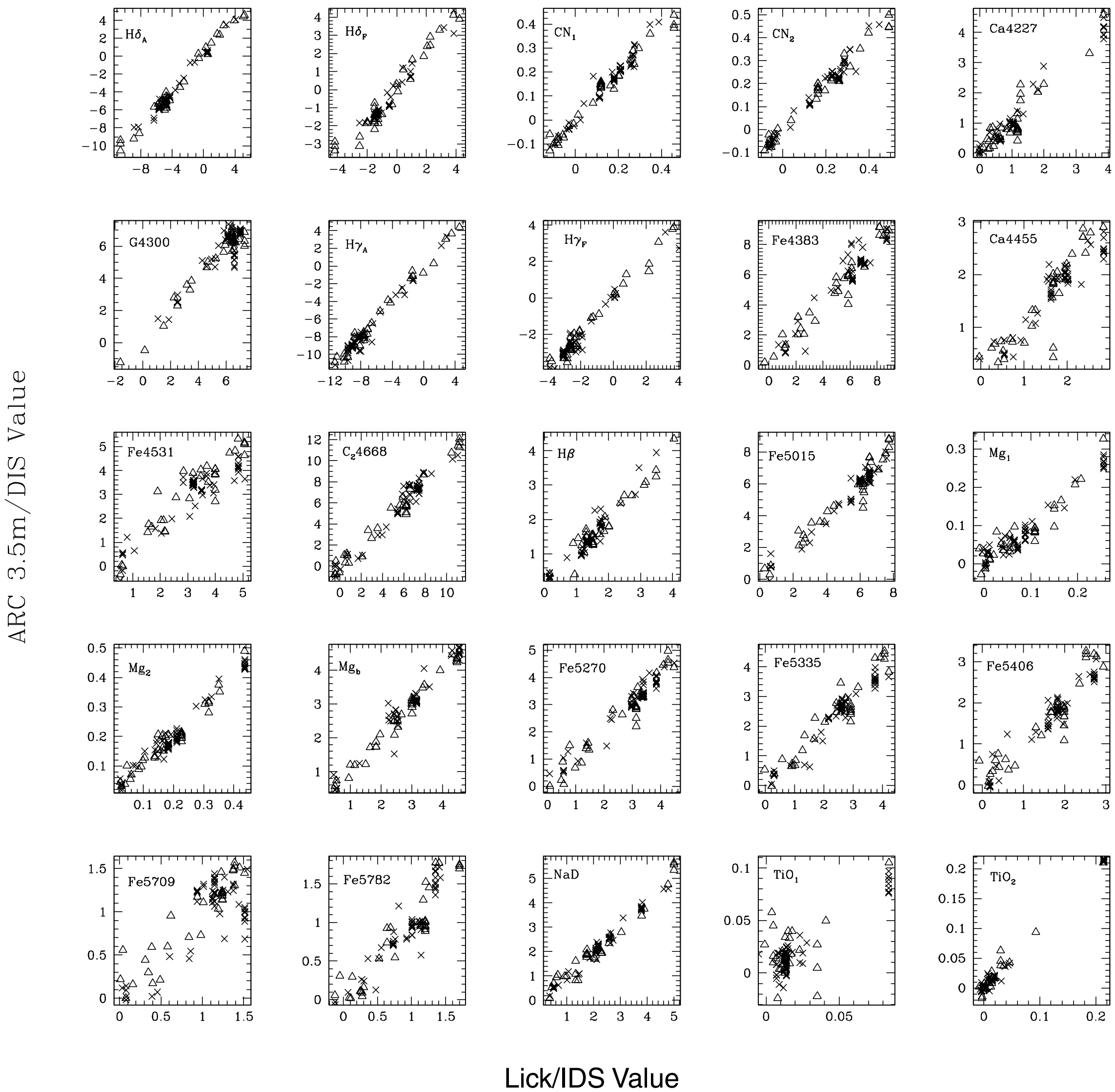

Figure 2. Comparison of indices obtained on standard stars using our instrument and using the Lick/IDS instrument. Each point is a Lick standard star. The triangles are DIS I. The crosses are DIS III. DIS III transformations were used for DIS II.

$$\mathrm{mag} = \frac{\mathrm{mag}_{\mathrm{raw}} + T_0 - T + B}{A},$$

where T_0 and T are the index values measured on the unbroadened and broadened templates, respectively (their ratio or difference is the velocity dispersion correction factor). The transformation terms A and B are given in Table 4 along with the rms scatter in applying the transformations to the stars. DIS III transformations were used for DIS II since the same gratings were used in both setups.

The flux response of the detector changes rapidly at the long-wavelength end of the blue channel, making measurements there difficult. Only the Mg_1 and Mg_2 indices were affected by this, but severely so, since their continuum bandpasses are far apart and the red continuum bandpass lies right where our flux response is steepest. This resulted in large scatter in the transformations of these indices. For the other indices, the scatter in the transformations is similar or slightly larger than that obtained by Proctor & Sansom (2002).

3.6 Comparison with the literature

Fig. 3 shows comparisons of Lick indices between this work and the most recently published values for NGC 4472. There is excellent agreement in the Ca4227, Hβ, Fe5015, ⟨Fe⟩, and Fe5270 profiles between this work and all the published values. Our other index profiles are systematically offset from at least one of the other two studies but the offset is within the uncertainties of transforming our data to the Lick system. In general, our results agree better with the long-slit data from Vazdekis et al. (1997) than the IFU data from Peletier et al. (1999). Nearly all our central values agree with those of Trager et al. Emission correction was not responsible for any disagreement among studies since NGC 4472 does not have much emission.

The first column of Fig. 4 shows index comparisons between this work (triangles), azimuthally averaged IFU data from Sil'chenko (1999; asterisks), and SAURON data extracted along the major-axis from Falcón-Barroso et al. (2004; squares) for NGC 7332.

Table 4. Transformations to the Lick/IDS system. The terms 'A' and 'B' are described in Section 3.5. 'rms' refers to the rms scatter in applying the transformations to the standard stars.

Index	DIS I A	DIS I B	DIS I rms	DIS II/III A	DIS II/III B	DIS II/III rms
$H\delta_A$	0.915	−0.198	0.615	0.872	0.620	0.385
$H\delta_F$	0.831	−0.215	0.518	0.854	0.247	0.297
CN_1	1.015	0.001	0.029	0.844	−0.005	0.022
CN_2	0.987	−0.007	0.025	0.830	−0.017	0.026
Ca4227	0.949	−0.013	0.384	0.726	−0.022	0.288
G4300	0.909	−0.868	0.501	0.741	−0.772	0.696
$H\gamma_A$	1.020	0.025	0.534	0.818	0.250	0.608
$H\gamma_F$	0.982	0.046	0.328	0.820	0.078	0.342
Fe4383	1.031	0.578	0.616	0.818	0.547	0.705
Ca4455	0.982	0.233	0.374	0.813	0.296	0.241
Fe4531	0.842	−0.381	0.549	0.856	−0.281	0.537
$C_2$4668	0.924	−0.748	0.652	0.879	−0.079	0.615
$H\beta$	1.060	−0.009	0.239	0.814	−0.298	0.200
Fe5015	0.911	−0.033	0.640	0.861	0.081	0.364
Mg_1	0.905	0.009	0.027	1.000	0.024	0.020
Mg_2	1.002	0.023	0.026	0.974	0.036	0.021
Mgb	1.047	0.107	0.157	0.825	−0.105	0.244
Fe5270	0.865	−0.239	0.372	0.888	0.238	0.230
Fe5335	0.813	−0.232	0.387	0.817	−0.415	0.244
Fe5406	0.864	−0.067	0.364	0.793	−0.107	0.222
Fe5709	0.975	−0.040	0.172	0.712	−0.475	0.322
Fe5782	0.774	−0.016	0.218	0.784	0.007	0.169
NaD	0.941	0.115	0.304	0.933	−0.181	0.142
TiO_1	1.317	0.015	0.021	1.035	0.014	0.010
TiO_2	0.868	−0.016	0.010	0.934	−0.010	0.006

All the central values are in agreement. The slope of our Hβ and Fe5270 profiles are steeper than Falcón-Barroso et al.'s but not as steep as Silchenko's. Our Mgb and Fe5015 profiles agree reasonably well with Falcón-Barroso's but Silchenko's Mgb profile is again steeper.

The second column of Fig. 4 shows index comparisons between this work, long-slit data from Fisher et al. (1996; crosses), IFU data from Sil'chenko et al. (2003; asterisks), and SAURON data from de Zeeuw et al. (2002; squares) for NGC 3384. Here also, Sil'chenko's profile is averaged azimuthally while de Zeeuw et al.'s is an extraction along the major-axis. This galaxy was observed on the night in which scattered light was corrected for as described in Section 3.2. Fisher et al.'s profiles are in good agreement with those from SAURON. Our Mgb and Fe5270 profiles agree marginally with published values. In the central regions, our Hβ profile falls in between de Zeeuw et al.'s and Sil'chenko et al.'s. Outside about 15 arcsec, our profile falls steeply, possibly due to inadequate scattered light correction, while de Zeeuw et al.'s stays flat. Our Fe5335 profile is much steeper than the published ones especially outside 15 arcsec (again likely due to inadequate scattered light correction).

The third column of Fig. 4 compares profiles for NGC 7457 with IFU data from Sil'chenko et al. (2002) and archival SAURON data which were also presented in Silchenko et al.'s paper. Silchenko et al.'s values are systematically smaller in the central regions than those obtained by others except for the case of Fe5335, where they are in agreement with ours. Our values have larger scatter but are otherwise in agreement with the SAURON values. The agreement among studies is worst for Hβ although this galaxy has little or no Balmer emission. The 2D SAURON map shows a negative gradient along the major-axis but not along the minor-axis, while Sil'chenko et al.'s 2D map shows no gradients whatsoever; our values are in better agreement with SAURON's than Sil'chenko et al.'s.

3.7 Absorption-line indices and SSP models

We have measured all 25 Lick indices in our galaxies as a function of galactocentric radius. In this paper, we concentrate on a subset of these indices which are sensitive to age, metallicity, and α/Fe. The most age-sensitive indices are the Balmer indices Hβ, Hγ_A, Hγ_F, Hδ_A and Hδ_F. Of these, Hβ suffers most from line-filling by emission, while the Hδ indices are the least affected. On the other hand, Hβ offers the most orthogonality with respect to metallicity-sensitive indices. Using a combination of the Balmer indices, we can obtain more reliable age estimates than with just one index. For metal lines, we compute the indices Mgb/$\langle$Fe$\rangle$ and [MgFe]' as discussed in Thomas, Maraston & Bender (2003, hereafter TMB); the former is directly related to α/Fe, and [MgFe]' traces metallicity without any sensitivity to α/Fe. Individually, [MgFe]' and the Balmer indices are degenerate in age and metallicity but together they can break the degeneracy since each index has a different age–metallicity dependence.

The integrated-light spectrum of an object is a linear combination of SSPs. Some objects, such as globular clusters, are well represented by a single SSP while galaxies are generally not. Still, one can characterize the SPs of a galaxy by an 'equivalent SSP'. Since the integrated light from a galaxy is weighted by luminosity, its SSP age and metallicity are likely to be different from the mass-weighted age and metallicity of its stars. SSP values are useful parametrizations of the SPs but cannot be interpreted as true ages and metallicities, since galaxies most likely contain a range of both. To avoid overinterpreting our data, we focus on the line strengths, mentioning SSP values only to illustrate dramatic differences between objects or regions within an object (i.e. 2 versus 10 Gyr as opposed to 8 versus 12 Gyr). Different line strengths in different objects (or within an object) imply different SPs; the SSP models allow us to infer the underlying source of the differences.

3.8 Bulge-to-disc decomposition

1D and 2D B/D was performed on our images. The disc and bulge were simultaneously fitted with an exponential and an $\exp(r^{1/n})$ profile, respectively. Initial fits were made using the fixed values of n of 1, 2, 3 and 4; the best fit of these was used as a starting guess in a final fit where n was allowed to vary as a free parameter. The results from the 1D decomposition were used as starting guesses for the 2D decomposition. In the 2D fits, both the bulge and disc components were allowed to be elliptical. This resulted in an overestimation of bulge size in most of our low-inclination barred galaxies (IC 302 and NGCs 266, 765, 3681, 3883 and 5375). A two-component bulge/disc model, such as ours, also overestimates the bulge component of our three S0s with luminous inner discs (NGCs 2787, 3384 and 3945) as previously found by Erwin et al. (2003). We pay close attention to these effects when studying the line-strength profiles in the bulge- and disc-dominated regions (Section 4.2). It was found through visual inspection that the best-fitting bulge and disc components of the other galaxies were reasonable. Fig. 5 shows the light profiles of our galaxies along with the best-fitting bulge and disc components.

The B/D used here primarily serves to determine the relative contribution of bulge and disc light as a function of radius; while B/D is notoriously difficult, especially when allowing for a Sersic

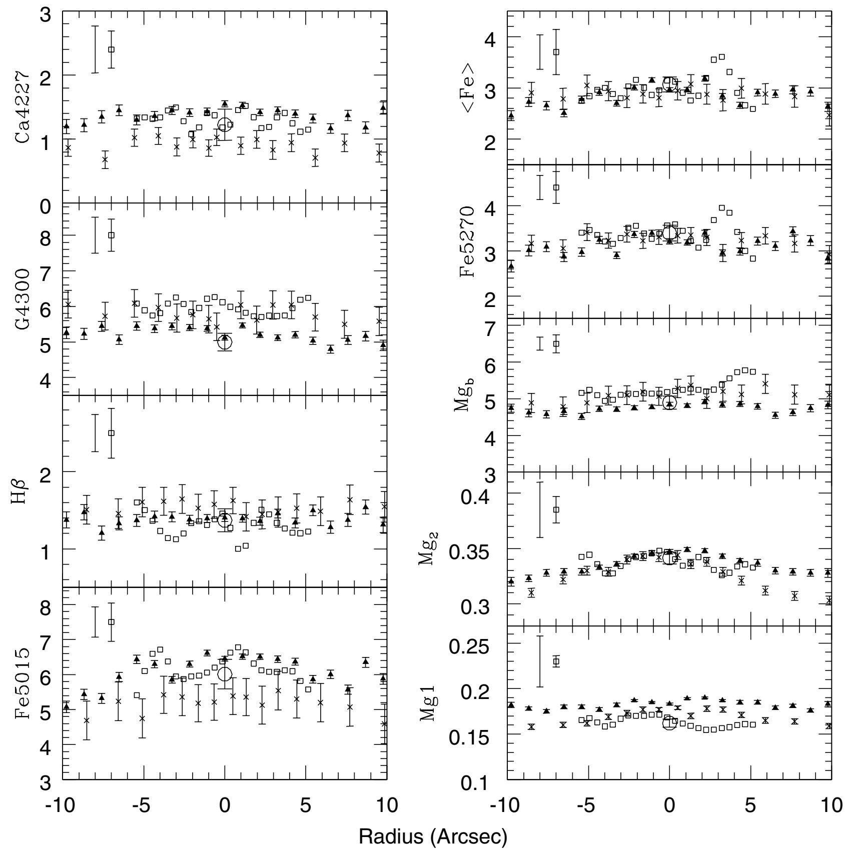

Figure 3. Comparison of line-strength gradients between this work and published values for NGC 4472. The triangles are from this work. The large circles are from Trager et al. (1998). The open squares are IFU data from Peletier et al. (1999) and the crosses are long-slit data from Vazdekis et al. (1997). At the top of each figure, the error bars without points represent the scatter in stars from our transformations to the Lick system; the error bars with squares indicate uncertainties in Peletier et al.'s data, including those involved in transforming to the Lick system.

bulge, this ratio is determined more robustly than the derived values of bulge effective radius and Sersic index.

Throughout this paper, the term 'disc' refers to the exponential outer region of the luminosity profile and the term 'bulge' refers to the excess light in the inner regions that was fitted with a Sersic profile. It is possible that these photometrically determined components do not correspond to a cold and a hot component, a flat and a spheroidal component, or a young and an old component. Through simulations, Abadi et al. (2003) found that while the stars of a simulated galaxy were well fitted by a Sersic + exponential profile, the hot and cold components were not well fitted individually by a Sersic and an exponential profile, respectively. Instead both were Sersic in the inner regions and exponential farther out. Using our kinematic information, we address this issue in Paper II. The structural properties and how they relate to the SPs will also be presented in that paper.

4 RESULTS

4.1 Central line strengths

Fig. 6 shows the measured central values of Hβ and [MgFe]' for our sample as well as published values for the MW (Puzia et al. 2002), M31 (Puzia et al. 2005), other bulges (Proctor & Sansom 2002) and elliptical galaxies (Trager et al. 1998; Proctor & Sansom 2002; Nelan et al. 2005). Symbol type and size denote Hubble type and central velocity dispersion, respectively. Most of Trager et al.'s and Proctor et al.'s ellipticals have large σ_0 but those of Nelan et al. (2005) populate all the σ_0 bins. Early- and late-type bulges preferentially populate the intermediate-σ_0 and small-σ_0 bins, respectively. S0s are found in all σ_0 bins. TMB's SSP models are superimposed on the plot. If a point has an accompanying vertical line segment, its location relative to the model grid was determined using an average of the other four Balmer indices instead of Hβ. The other end of the line segment shows the Hβ value. If the difference between these is large, this is due most likely to errors in Hβ emission correction since the galaxies whose Hβ values lie outside the model grid have strong Hβ emission. Two galaxies have Hβ values that put them outside the plot range. These are NGCs 2787 and 5719 with Hβ values of −0.506 and 0.607, respectively. If a point does not have an accompanying vertical line segment, its location relative to the model grid does not change much depending on which Balmer index is plotted versus [MgFe]'.

Our central indices were measured on spectral extractions binned to match Trager et al.'s 1.4 × 4-arcsec^2 aperture and Proctor et al.'s 1.25 × 3.6-arcsec^2 aperture as closely as possible (1.5 × 3.3, 1.5 × 4.2 and 1.5 × 3.8 arcsec^2 for DIS I, II and III, respectively). Nelan et al. used 2-arcsec-diameter fibres. Nelan et al.'s large-σ_0 galaxies have systematically smaller [MgFe]' than those of Trager et al. and Proctor et al. Line-strength gradients are likely to be responsible for the offset. While the three studies used similar angular apertures, Nelan et al.'s galaxies are considerably more distant ($cz \sim$15 000 km s^{-1} for Nelan et al., 3000 km s^{-1} for Trager et al., and 2000 km s^{-1} for Proctor et al.). Since Nelan et al. sampled a larger portion of each

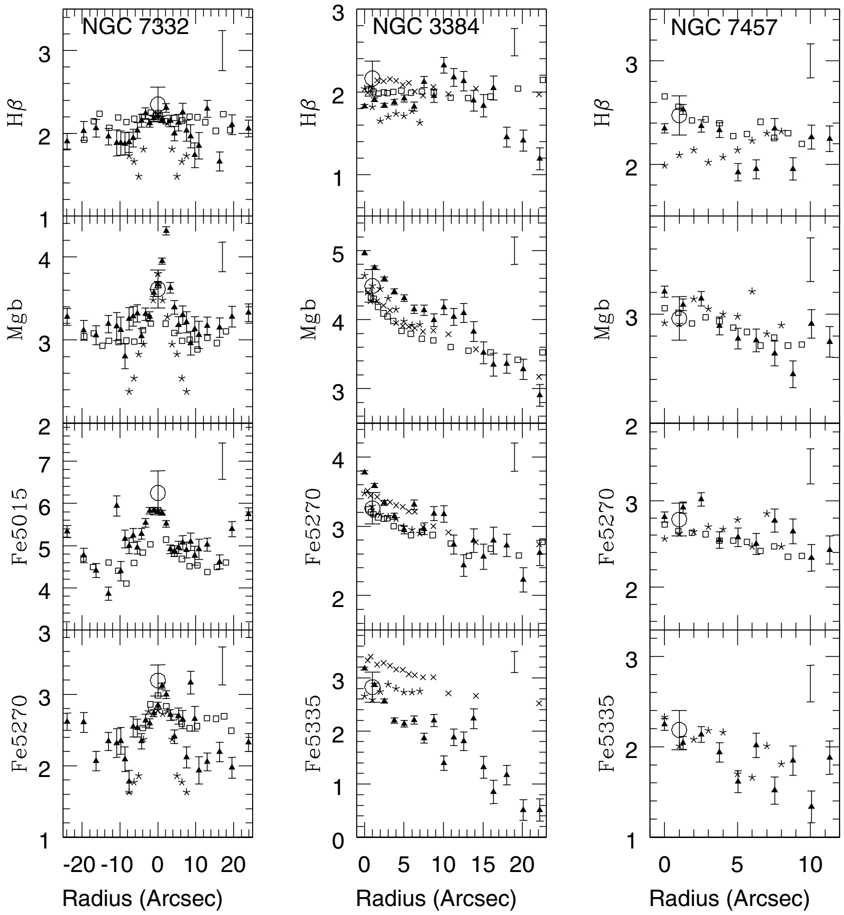

Figure 4. Comparison of line-strength gradients between this work and published values for NGCs 7332, 3384 and 7457. The triangles are from this work. The asterisks are azimuthally averaged IFU data from Sil'chenko (1999), Sil'chenko et al. (2003), and Sil'chenko et al. (2002) for NGCs 7332, 3384 and 7457, respectively. The squares are SAURON data extracted along the major-axis from Falcón-Barroso et al. (2004), de Zeeuw et al. (2002) and Sil'chenko et al. (2002). For NGC 3384, the crosses are long-slit data from Fisher et al. (1996).

galaxy and since early-type galaxies have decreasing [MgFe]' with radius, we would expect them to obtain smaller 'central' values for [MgFe]'. Kuntschner et al. (2006) computed aperture corrections to Mgb and Fe5015 in early-type galaxies and found the magnitude of the correction to be similar in these two indices. Assuming that Nelan et al.'s galaxies are a factor of 5 farther than those of Trager et al. and assuming that [MgFe]' has a similar correction as Mgb and Fe5015, yields an [MgFe]' value of 3.8 for Nelan et al.'s largest-σ_0 bin. This brings its SSP metallicity close to those of the large-σ_0 ellipticals from Trager et al. and Proctor et al.

Bulges can be broadly classified into three groups according to which region of Fig. 6 they populate: the old metal-rich (OMR, lower right-hand panel) region, the young metal-rich (YMR, upper right-hand panel) region with ages less than 3 Gyr and supersolar metallicity, or the metal-poor (MP, left-hand panel) region with subsolar metallicity. This classification scheme is analogous to that of Prugniel et al. with our MP, OMR and YMR classes corresponding to their A, B and C classes, respectively. The bulges of the MW and M31 lie in the MP region.

Membership in a region is closely related to bulge colour. Most of the red bulges populate the OMR region while all but one of the bulges in the MP region are blue. The exception is IC 267 (the red open square with [MgFe]' = 1.65). This bulge has strong Balmer emission which suggests that its red colour is due to dust from recent star formation as opposed to an old SP. Colour does not uniquely represent the SPs of blue bulges; some bulges are blue because they are metal poor while others are blue because they are young. To distinguish the two classes of blue bulges in subsequent plots, the MP bulges are marked with an additional blue dot.

Besides colour, central line strengths are sensitive to Hubble type. All the early-type (S0–Sab) bulges have large central metallicities. The blue early types are in the YMR region, while the red early types are in the OMR region. Bulges of late-type spirals are more heterogeneous in their central line strengths than those of early types. The MP region is populated exclusively by late types, but late types are also found in the other two regions. Ellipticals populate all three regions of the plot.

Much of the variation in central line strengths is due to correlations between the line strengths and the global kinematics. The largest-σ_0 galaxies, which include a large fraction of Trager et al.'s and Proctor et al.'s ellipticals, exclusively populate the OMR region. As σ_0 decreases, SSP age and SSP metallicity decrease in Nelan et al.'s ellipticals; this appears to be true in our bulges and those of Proctor et al. as well but at fixed σ_0, the scatter in SSP age and SSP metallicity among bulges is large. Caldwell et al. (2003) also found that small-σ_0 ellipticals have, on average, smaller SSP ages and metallicities than large-σ_0 ellipticals; unfortunately, we cannot include their data in Fig. 6 because they did not measure the

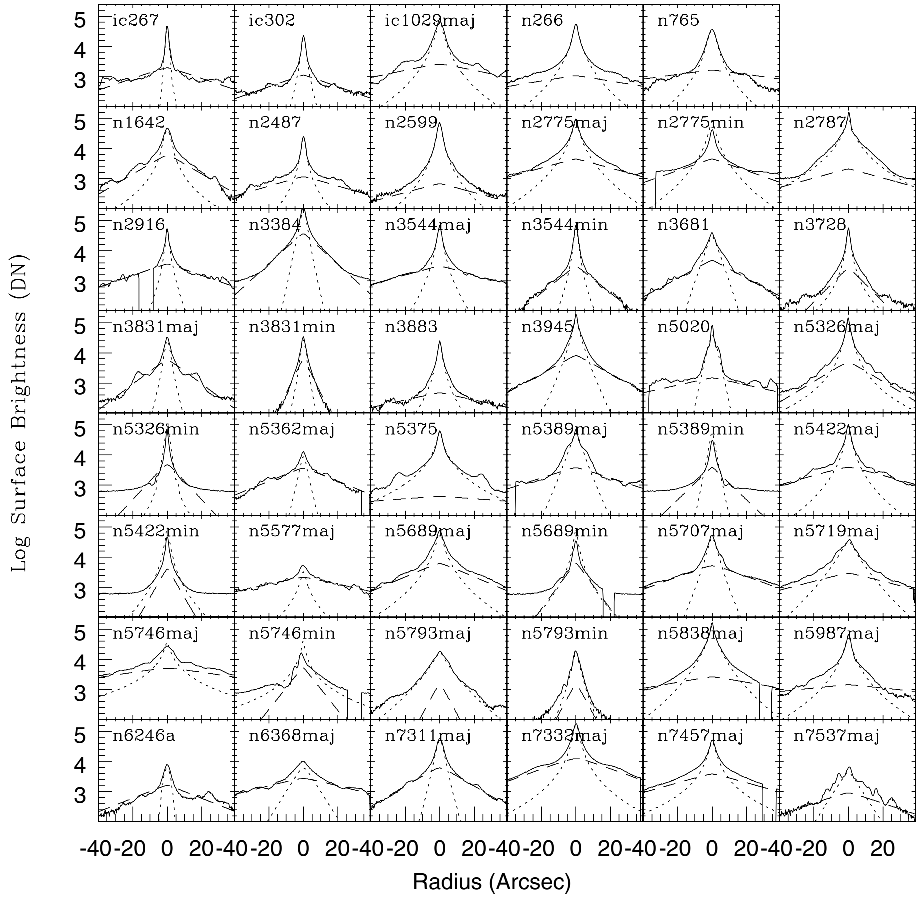

Figure 5. Results of 2D B/D. The light profile of each galaxy is shown as a solid line, the best-fitting bulge as a dotted line, and the best-fitting disc as a dashed line. The position angles are the same as those used for the spectroscopy (Table 3).

same indices. The OMR region is populated almost exclusively by large-σ_0 [$\log(\sigma_0) > 2.2$] galaxies, while the MP region is populated exclusively by small-σ_0 [$\log(\sigma_0) < 2$] galaxies. The YMR region is populated by small- and intermediate-σ_0 galaxies.

The different types of bulges (MP, YMR and OMR) and ellipticals form a continuous and overlapping sequence on a plot of [MgFe]' versus central velocity dispersion (Fig. 7, top left-hand panel). In both bulges and ellipticals, [MgFe]' is correlated with σ_0 at the low-σ_0 end. As σ_0 increases beyond $\log(\sigma_0) > 2.2$, [MgFe]' remains constant. Bulges show larger scatter than ellipticals in the [MgFe]'–σ_0 relation.

[MgFe]' is also correlated with the maximum disc rotational velocity (Fig. 7, top right-hand panel), as previously found by Prugniel et al. However, the blue bulges with $\log V_{\rm max} > 2.2$ are significant outliers in the [MgFe]'–$V_{\rm max}$, having smaller central values of [MgFe]' than their red counterparts.

Balmer indices are anticorrelated with σ_0 and weakly anticorrelated with $V_{\rm max}$ (middle panel of Fig. 7). Residuals in the Hβ–σ_0 and Hβ–$V_{\rm max}$ relations are correlated with colour such that at a given σ_0 and $V_{\rm max}$, blue bulges have larger Hβ values than red bulges.

At fixed σ_0, age and metallicity are known to be anticorrelated in ellipticals (Trager et al. 2000b; Proctor & Sansom 2002), a result which has important consequences for the origin of the red sequence (See Section 5.1). This is clearly seen in Fig. 6. Nearly all the green and magenta crosses belong to the two largest-σ_0 bins. Of these, the ones with the largest SSP age ($\sim$15 Gyr) have the smallest SSP metallicity ([Z/H] $\sim$ 0.2), while those with the smallest SSP age ($\sim$3 Gyr) have the largest SSP metallicity ([Z/H] $\sim$ 0.7). A similar anticorrelation does not appear to exist for bulges; if it does exist, there is considerably larger scatter than in ellipticals.

In bulges and ellipticals, the α/Fe ratio as indicated by Mgb/$\langle$Fe$\rangle$, is correlated with σ_0 and $V_{\rm max}$ (bottom panel of Fig. 7). In these two plots, the region within the inner horizontal lines corresponds to models with solar α/Fe for metallicities $-1.35 \leqslant$ [Z/H] $\leqslant 0.35$ and ages from 8 to 15 Gyr; the region within the outer lines represents models with the same metallicities and ages from 3 to 15 Gyr (from fig. 4 of TMB). Red bulges and ellipticals show good overlap in the Mgb/$\langle$Fe$\rangle$–σ_0 diagram. With a few exceptions, blue bulges are consistent with having solar α/Fe. Consequently, most blue bulges have smaller Mgb/$\langle$Fe$\rangle$ ratios than red bulges or ellipticals at a given value of σ_0 or $V_{\rm max}$. One of the blue bulges, NGC 6246A, has supersolar α/Fe, large age, and small metallicity ([Z/H] ~ -0.8) like MW halo stars. The other two blue bulges with supersolar α/Fe have supersolar metallicity like the majority of red bulges.

There are hints of possible differences between barred and unbarred galaxies in some of the scaling relations. At fixed σ_0 and $V_{\rm max}$, barred galaxies appear to have larger central values of [MgFe]' than unbarred galaxies (or galaxies with elliptical-shaped bulges). b/p bulges generally lie between and exhibit larger scatter than barred and unbarred/elliptical bulges in the [MgFe]'–σ_0 and [MgFe]'–$V_{\rm max}$ diagrams. The central regions of b/p bulges could be contaminated by the foreground disc resulting in smaller values of [MgFe]' than those of the low-inclination barred galaxies. Barred galaxies appear to have smaller Hβ than unbarred galaxies at fixed σ_0 and $V_{\rm max}$. No striking difference is seen between barred and unbarred galaxies in the scaling relations involving Mgb/$\langle$Fe$\rangle$. Note that the parame-

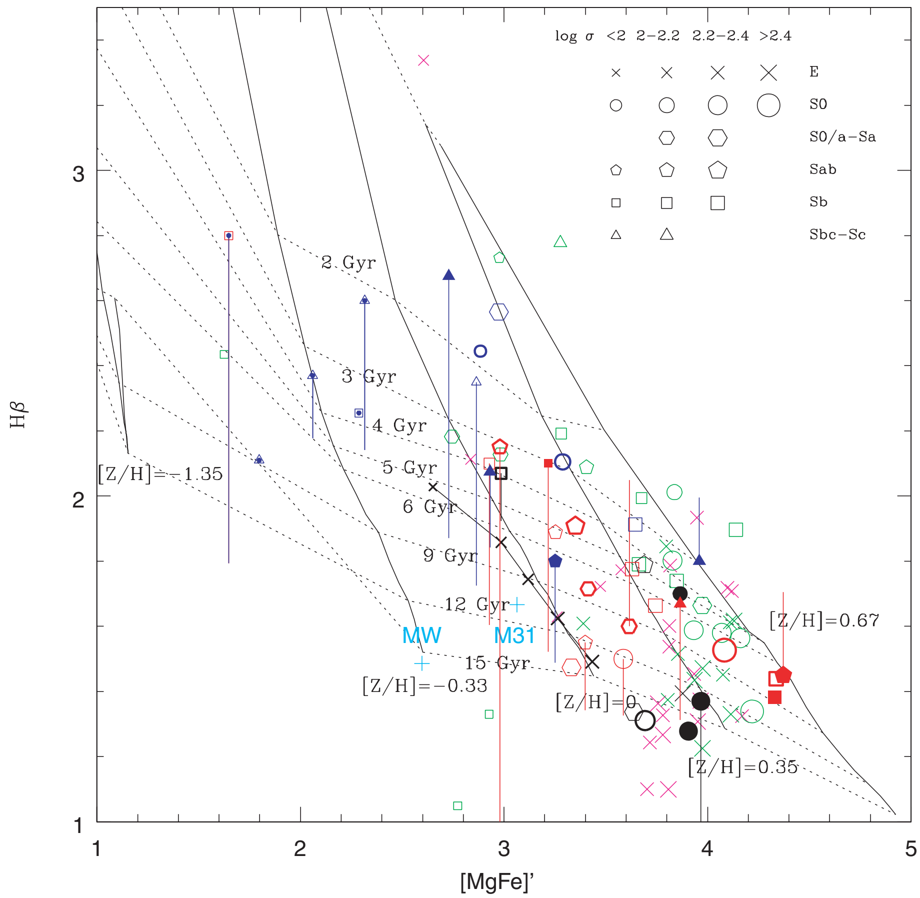

Figure 6. Hβ versus [MgFe]' in the central regions of bulges and ellipticals. Symbol type and size denote Hubble type and central velocity dispersion, respectively, as shown in the legend. The bold black crosses connected by lines are from Nelan et al. (2005). Each bold cross represents the mean of approximately 700 early-type galaxies. The magenta crosses are galaxies from Trager et al. (1998) that were classified as elliptical and had Hβ uncertainty less than 0.2 and velocity dispersion uncertainty less than or equal to 10 km s^{-1}. The green symbols are bulges and ellipticals from Proctor & Sansom (2002). The MW (Puzia et al. 2002) and M31 (Puzia et al. 2005) are shown as '+' symbols. Bulges from this work are shown in blue or red as in Fig. 1 or in black if no colour information is available. As in Fig. 1, the filled symbols are barred galaxies, the thick open symbols are b/p bulges, and the thin open symbols are unbarred galaxies or elliptical-shaped bulges. Our five metal-poor (MP) bulges are marked with an additional blue dot. TMB's models are superimposed on the plot. If a point has an accompanying vertical line segment, its location relative to the model grid was determined using an average of the other four Balmer indices, instead of Hβ. The other end of the line segment shows the Hβ value. If a point does not have an accompanying vertical line segment, its location relative to the model grid does not change much depending on which Balmer index is plotted versus [MgFe]'.

ter space defined by morphology, kinematics, and dynamics is only sparsely sampled in this study. A considerably larger galaxy sample is required to definitively determine whether or not barred and unbarred galaxies follow the same scaling relations.

The central regions of our three barred S0s with disc-like structure and kinematics (filled black circles) have supersolar SSP metallicities and α/Fe ratios and two of the three have large SSP ages. If all discs formed stars on long time-scales (several Gyr), we would expect them to have small α/Fe ratios, like the MW disc at the solar neighbourhood, since interstellar medium (ISM)-enrichment would eventually be dominated by SNe Ia. The 'luminous inner discs' of these S0s have not had such a star formation history. Peletier et al. (1999) found that the Sombrero galaxy is also dominated by a fast rotating disc whose [Mg/Fe] is similar not to other discs but to ellipticals of similar mass as the Sombrero.

4.2 Line-strength gradients

Figs 8 and 9 show [MgFe]' profiles in our galaxies. The open squares and filled triangles show points that were and were not corrected for [N I] 5199 emission, respectively; the correction was seldom performed. The solid and dotted vertical lines indicate where the ratio of bulge to disc light is 2 and 1/2, respectively, as determined from the B/D. We performed linear least-squares fits to the [MgFe]' profiles separately in the bulge- and disc-dominated regions, selecting the points to include based on the B/D but making exceptions where they seemed appropriate (such as when the bar was fit as a bulge; see Section 3.8). We usually avoided the transition region from bulge to disc dominance. The best-fitting lines are shown in red. The discrepancy due to scattered light between our Fe5335 profile of NGC 3384 and published ones (see Section 3.6) does not affect [MgFe]' significantly. The [MgFe]' profile obtained by Fisher et al. (1996) for NGC 3384 (green curve in Fig. 8) shows good agreement with ours.

Most galaxies have negative [MgFe]' gradients (decreasing [MgFe]' with increasing radius) in the bulge-dominated region. [MgFe]' generally decreases steadily from the galaxy centre to the solid vertical lines, beyond which the slope of the profile changes. In low-inclination galaxies and along the major-axes of inclined galaxies, [MgFe]' is usually larger just outside the solid vertical lines than

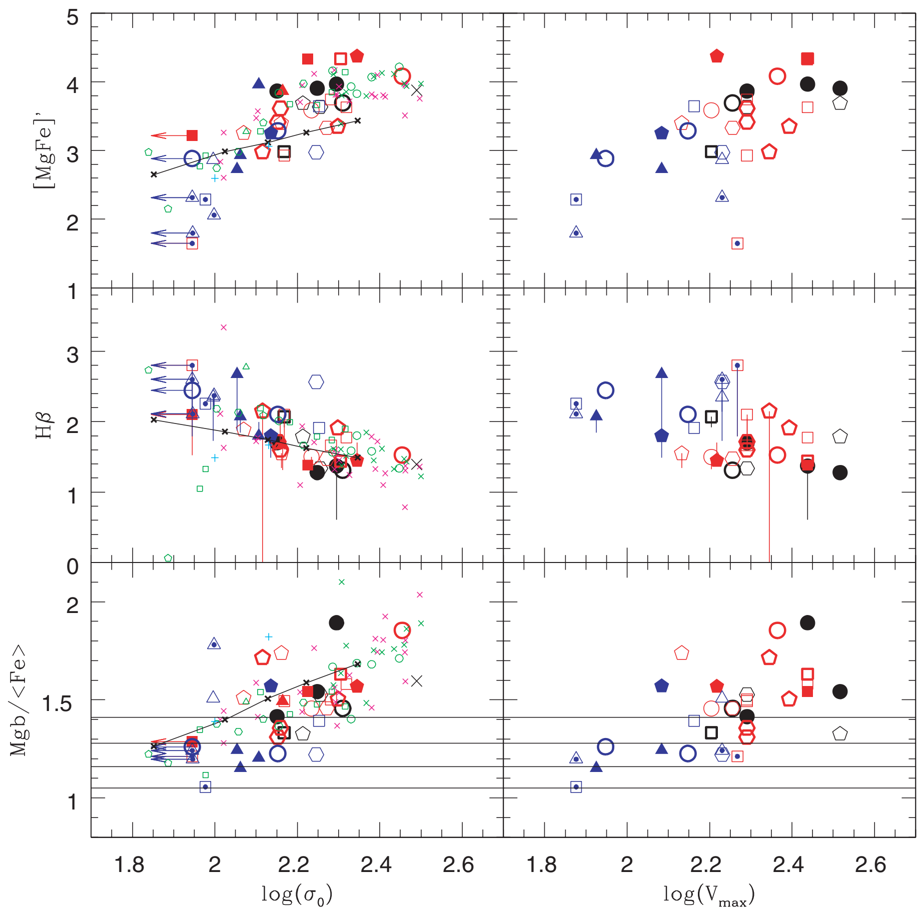

Figure 7. Central line strengths versus central velocity dispersion and maximum disc rotational velocity. The symbols are as in Fig. 6, except that the large symbols represent values obtained in this work and the small symbols represent published values. The arrows represent upper limits for galaxies whose velocity dispersions are close to or below our resolution limit. IC 302 and NGCs 765, 2487, 2916 and 6246A are not shown on the right-hand panel, since their inclinations are too low to measure rotation. In the bottom panel, the region within the inner horizontal lines corresponds to models with solar α/Fe for metallicities $-1.35 \leqslant [Z/H] \leqslant 0.35$ and ages from 8 to 15 Gyr (from fig. 4 of TMB). The region within the outer horizontal lines represents models with the same metallicities and ages from 3 to 15 Gyr.

inside it (NGC 5987 is a good example), suggesting that the outer bulge has a smaller line strength than the inner disc. The fact that we can identify distinct bulge and disc components in the [MgFe]' profiles suggests that disc contamination is not significant within the solid vertical lines.

The galaxies that do not have negative [MgFe]' gradients in the bulge-dominated region are generally those with small bulges (solid vertical lines are located at a radius of less than 5 arcsec). In four of these (IC 267 and NGCs 3831, 5577 and 6246A), there is the hint of a positive gradient while the rest (NGCs 2916, 5362 and 6368) are consistent with having little or no gradient. Since the profiles are always different inside and outside the solid lines, they cannot be explained by disc contamination. Two galaxies with larger bulge-dominated regions, NGCs 3681 and 5707, also do not have negative [MgFe]' gradients in the bulge. They do, however, have a negative gradient in the transition region from bulge to disc dominance.

Another test for disc contamination is how the major- and minor-axis profiles vary as a function of inclination. Low-inclination galaxies should have identical profiles if there are no azimuthal differences in line strengths. The major- and minor-axis profiles of NGC 2775, the only low-inclination galaxy for which both were obtained, are indeed identical. At intermediate inclinations, one expects more disc contamination on one side of the minor-axis (the dusty side) than the major-axis for the same solid angle. In the three intermediate inclination galaxies for which we have major- and minor-axis spectra (NGCs 3544, 5326 and 5389), this effect is clearly seen; the minor-axis profile is asymmetric outside the solid vertical lines with the profile turning over at a smaller galactocentric distance on the dusty (left hand) side than that on the dust-free side. Within the solid lines, there is good agreement in gradient slopes between major- and minor-axes, indicating that disc contamination is not significant. In edge-on galaxies, it is difficult to estimate the degree of disc contamination in the central region; but away from the centre, there is more disc contamination along the major-axis than along the minor-axis. In two of our edge-on galaxies (NGCs 5422 and 5689), the minor-axis profile continues to decrease beyond the distance at which the major-axis profiles turn over briefly (due to the inner disc having larger [MgFe]' than the outer bulge, as discussed above). The profiles of our other two edge-on galaxies (NGCs 5746 and 5793) are too noisy to determine if this effect is present. Previously, Fisher et al. (1996) noted differences in major- and minor-axis index profiles in S0s, with the major-axis profiles flattening off at large radii, while the minor-axis profiles continue to decrease.

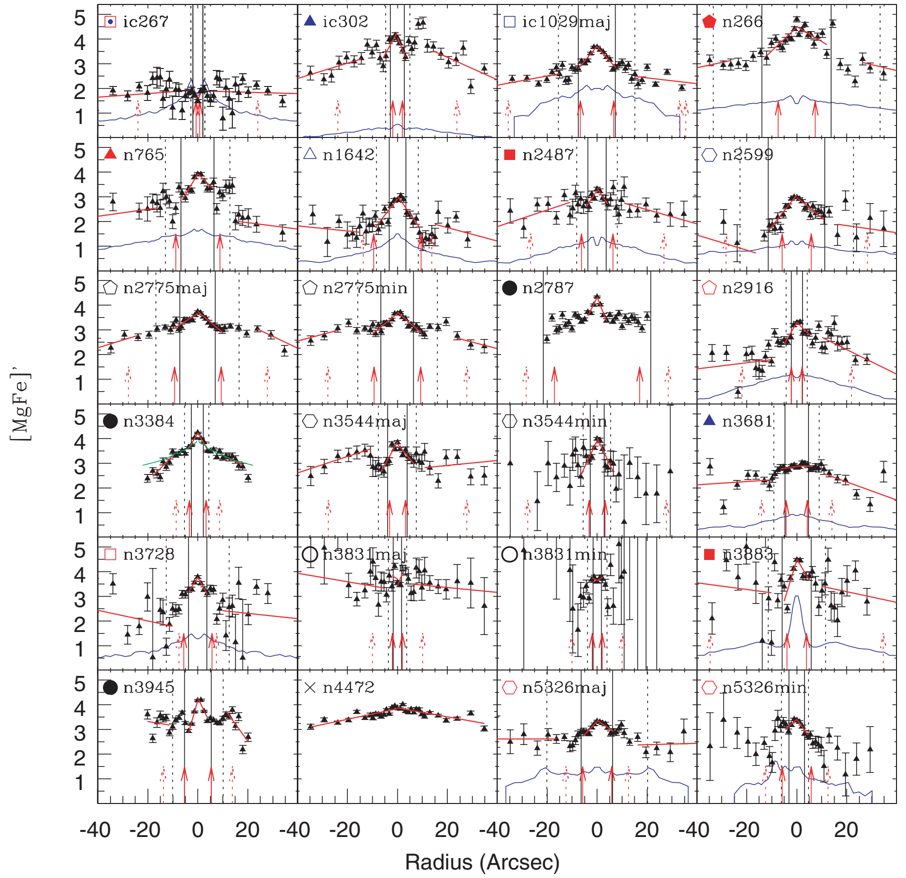

Figure 8. [MgFe]' profiles in our galaxies. The open squares and filled triangles show points that were and were not corrected for [N I] 5199 emission, respectively. For NGC 3384, the green curve shows the profile obtained by Fisher et al. (1996). At the top left-hand side of each plot are symbols denoting the galaxy type (as in Fig. 6) as well as the NGC or IC identifiers. The solid and dotted vertical lines indicate where the ratio of bulge to disc light is 2 and 1/2, respectively, as determined from the B/D. The solid and dotted red arrows indicate the location of the bulge effective radius and disc scalelength, respectively. Results from linear least-squares fits performed separately in the bulge- and disc-dominated regions are shown in red. The blue lines are colour profiles ($B - K - 3$) from PB and DJ. $B - K$ was not available for IC 302; $V - H - 3$ is shown instead.

The slopes of [MgFe]' gradients within the bulge along the major-axis are shown in Fig. 10 as a function of the central [MgFe]', central velocity dispersion, and maximum disc rotational velocity. Galaxies with large central values have correspondingly large negative gradients, while the three galaxies with the smallest central values, namely IC 267 and NGCs 5577 and 6246A, have positive gradients. Gradients are weakly correlated with the global kinematics, perhaps slightly more tightly with $V_{\rm max}$ than with σ_0. Proctor (2002) also found that index gradients in bulges were correlated with central velocity dispersion and more tightly with central indices. It does not appear as if the tightness of the correlation between gradients and the global kinematics would improve if some Hubble types (for instance, early types) were excluded but this result needs to be confirmed with a larger galaxy sample.

Most galaxies also have negative gradients in the disc-dominated region but it is shallower than that of the bulge. Some galaxies (e.g. NGCs 5746, 5838 and 7332) have no gradient in the disc.

The [MgFe]' value at one disc scalelength (computed using the results of our least-squares fits) is correlated with the central value (Fig. 11). This indicates that the metallicity of the disc is correlated with that of the bulge. This correlation holds for all galaxies, not just the late types or those with bars, blue bulges, or bulges identified as having disc-like structural or kinematical properties.

4.2.1 Separating age and metallicity effects

Figs 12 and 13 show gradients in the Hδ_A index. The Hδ profiles show less scatter than the lower-order Balmer indices since they are less affected by emission. The squares and filled triangles show points that were and were not corrected for emission, respectively. Least-squares fits were performed on the Balmer indices exactly in the same manner as for the [MgFe]' profiles. The fit results for Hδ_A are shown in red in Fig. 12. Gradient slopes computed on individual indices were combined to disentangle the effects of age and metallicity. This is shown in Fig. 14 for the [MgFe]'–Hδ_A index combination. A red arrow is drawn from the galaxy centre to the edge of the bulge-dominated region (on either side of the galaxy) and a blue arrow is drawn from there to the disc scalelength.

The majority of galaxies (at least 29 out of 38) have negative metallicity gradients in the bulge-dominated region. NGCs 3681, 3831, 5362, 5707 and 7311 show little or no metallicity gradient in the bulge. Three of the five MP bulges (IC 267 and NGC 5577 and 6246A) have positive metallicity gradients. The remaining two galaxies (NGCs 5746 and 5793, both edge-on with b/p bulges) show internal discrepancies in the fit results. Except for its minor-axis Hδ_A profile, NGC 5746 is consistent with having little or no metallicity gradient. The minor-axis profiles of NGC 5793 consistently

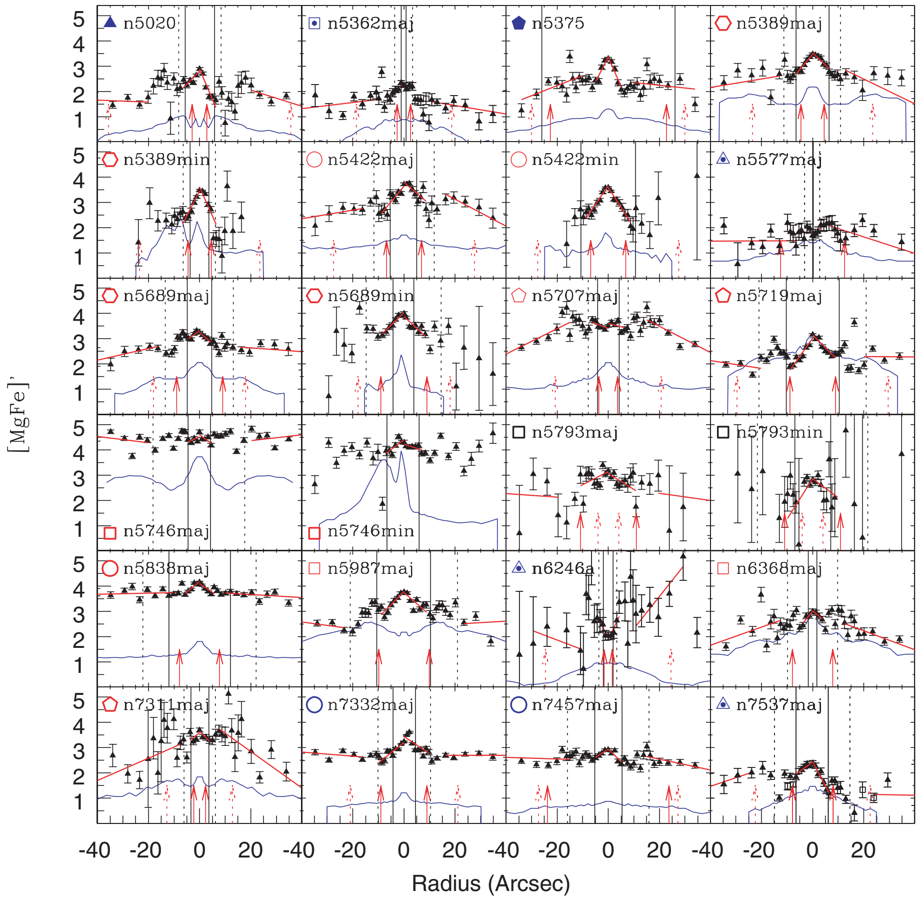

Figure 9. [MgFe]' profiles in our galaxies (continued). The symbols are as in Fig. 6.

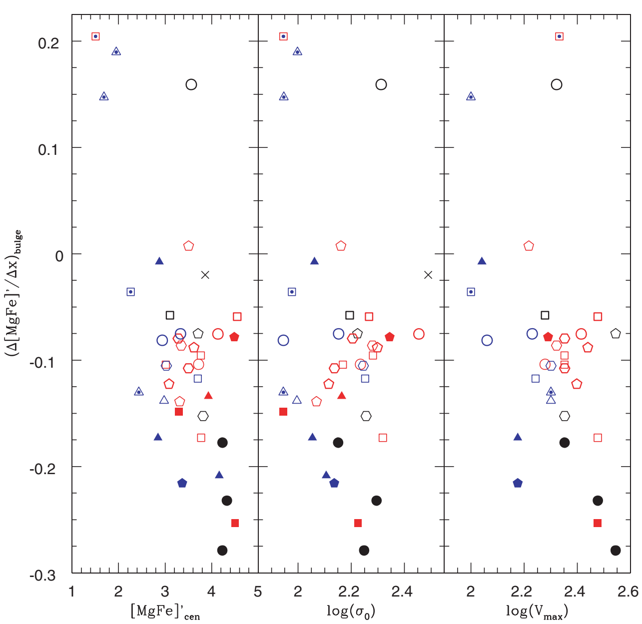

Figure 10. [MgFe]' gradient within the bulge-dominated region versus the central value of [MgFe]', central velocity dispersion, and maximum disc rotational velocity. For galaxies with major- and minor-axis observations, the gradient along the major-axis is shown. The symbols are as in Fig. 6.

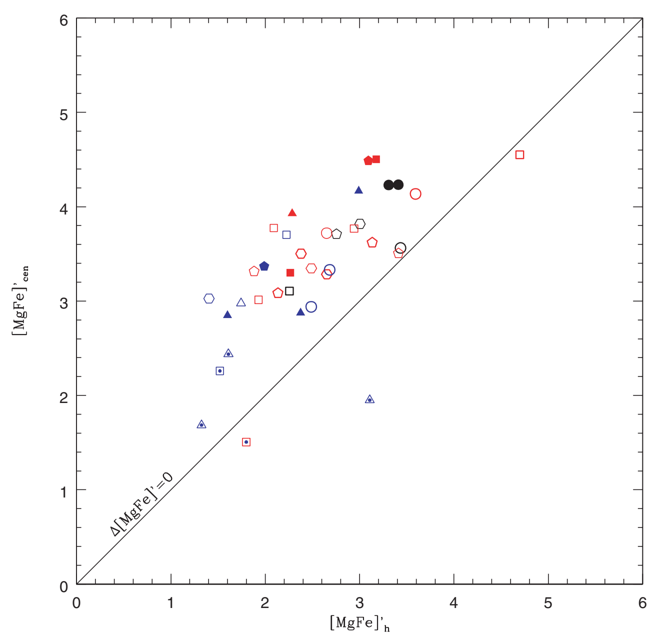

Figure 11. The central value of [MgFe]' versus the value at one disc scale-length computed using the results from a least-squares fit to the [MgFe]' profiles. The solid line shows where objects would lie if their bulges and discs were identical in [MgFe]'. The symbols are as in Fig. 6.

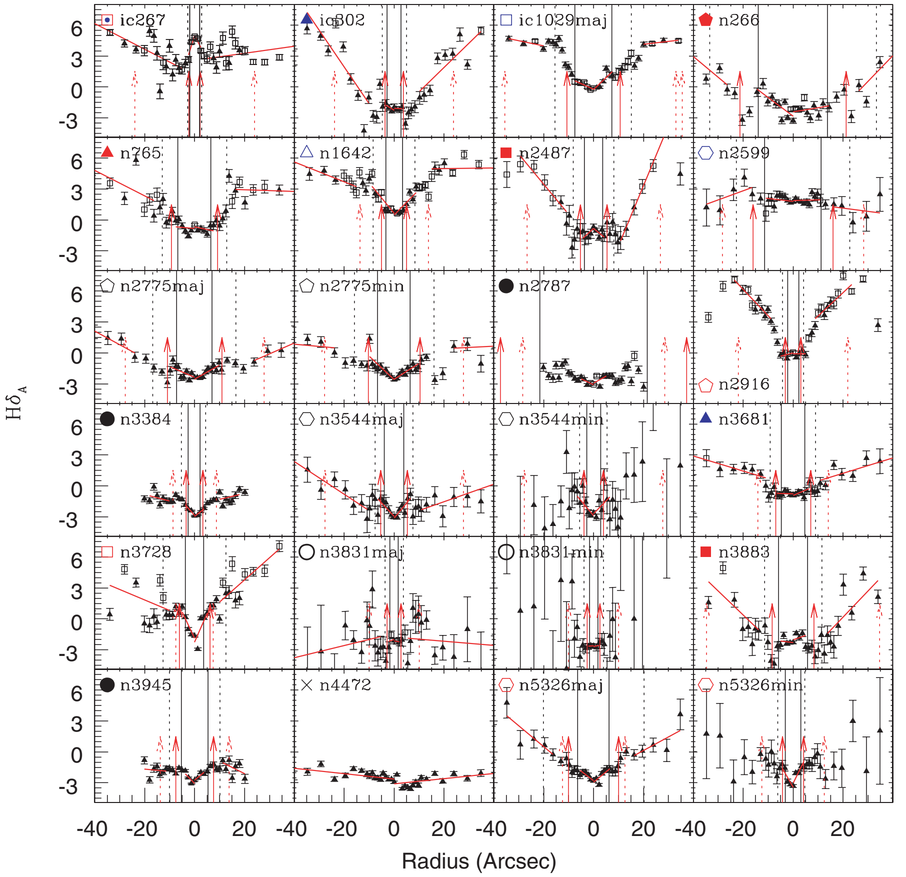

Figure 12. Hδ_A profiles in our galaxies. The symbols are as in Fig. 6.

show a negative metallicity gradient but the major-axis profiles show none.

The majority of galaxies are consistent with having little or no age gradient within the bulge. At least 10 galaxies (IC 302 and NGCs 266, 765, 2487, 2599, 2916, 3883, 5020, 5375 and 5838) have a positive age gradient (larger age with increasing radius). Of these, seven are barred and one has a b/p bulge. At least five galaxies (NGCs 3728, 5577, 6246A, 7311, and the major-axis of NGC 5793) have a negative age gradient in the bulge.

The Balmer indices show large scatter in the disc-dominated regions, making it difficult to determine whether metallicity and age gradients are present. Plots of gradients in the five Balmer indices versus [MgFe]' (such as Fig. 14) do not show consistent results for approximately half the galaxies. Of the other half, most have a negative age gradient and little or no metallicity gradient. Most discs are solar or subsolar in metallicity but NGCs 5746 and 5838 are supersolar well into the disc-dominated region.

4.2.2 Comparison with colour gradients

The blue lines in Figs 8 and 9 are colour profiles ($B - K - 2$) from PB and DJ. The shapes of the [MgFe]' and colour profiles agree often but not always. Where discrepancies exist, they can usually be explained, at least qualitatively, by differences in age- and metallicity-sensitivity between [MgFe]' and $B - K$ colour, with $B - K$ being more age-sensitive. For instance, NGC 266, 2487, 2916 and 3728 show a positive colour gradient but a negative [MgFe]' in the central 5 arcsec. Of these, NGCs 266 and 2487 show a negative Hδ_A gradient in the central region which indicates a positive age gradient (a negative Hδ_A gradient could also be caused by a positive metallicity gradient but that is ruled out by the negative [MgFe]' gradient). NGC 2916's Hδ_A profile is flat in the central 5 arcsec which, combined with its negative [MgFe]' gradient, also indicates a positive age gradient. A negative metallicity gradient combined with a positive age gradient can explain the differences in [MgFe]' and colour gradients in these galaxies. This explanation is not satisfactory for NGC 3728 whose [MgFe]' and Balmer profiles suggest a negative metallicity gradient and little or no age gradient, while its colour profile suggests a positive gradient in age, metallicity, or both.

De Jong (1996b) noted that it is not possible to identify distinct bulge and disc components using the colour profiles. However, it is possible to do so using the [MgFe]' profiles. As mentioned earlier, the slopes of the [MgFe]' profiles are almost always distinct inside and outside the bulge-dominated region, with the former usually having a steeper negative gradient. Eleven out of the 14 DJ galaxies and 15 out of the 17 PB galaxies have negative [MgFe]' gradients in the bulge-dominated region. The majority of the PB galaxies (12 out of 17 as opposed to four out of the 14 DJ galaxies) also show a negative colour gradient in the bulge-dominated region. The systematic difference in colour gradients between the PB and DJ samples is likely due to different amounts of extinction at different inclinations since the PB galaxies have large inclinations while the DJ galaxies have small ones.

If we compare the gradient in [MgFe]' from the galaxy centre to the disc scalelength (computed using the fit results) with the colour gradient (read from the profiles), we find that these two quantities are not tightly correlated (Fig. 15). This could be due to a combination

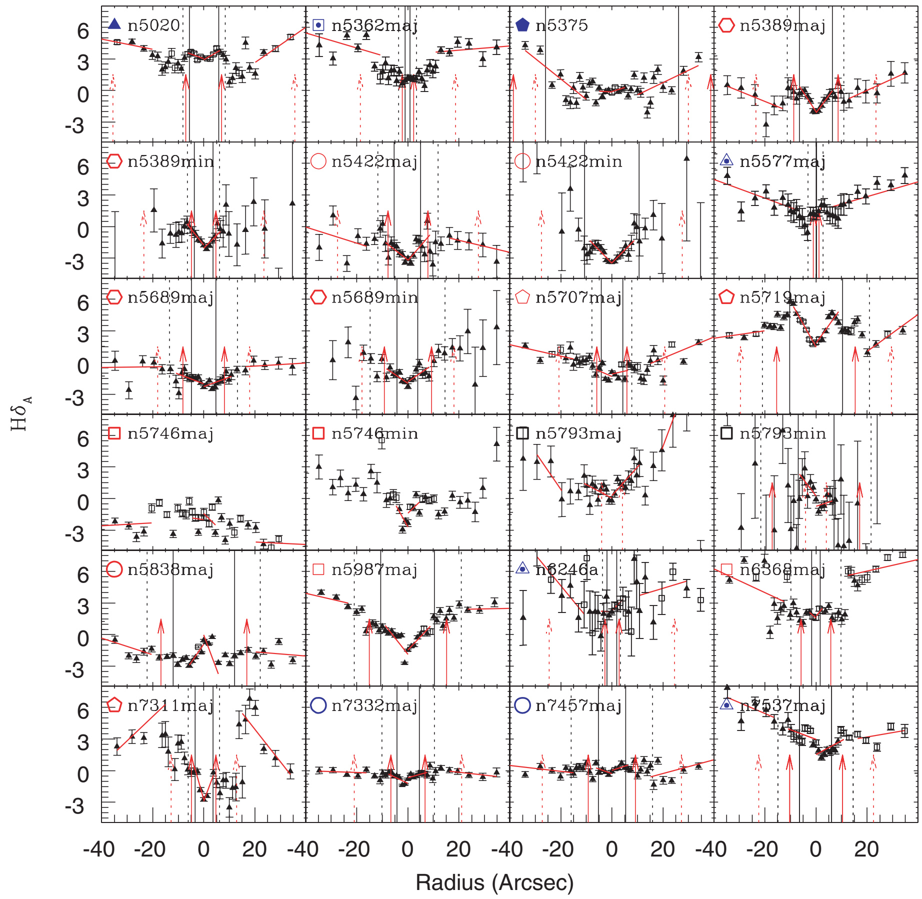

Figure 13. Hδ_A profiles in our galaxies (continued). The symbols are as in Fig. 6.

of different age–metallicity sensitivities between [MgFe]' and $B-K$ colour and the influence of dust on the colour profiles.

Gadotti & dos Anjos (2001) found a greater prevalence of null or positive colour gradients in barred galaxies than in unbarred galaxies. They interpreted their result as evidence for gradients being erased by bar-driven mixing. We do not see any systematic difference between barred and unbarred galaxies with regard to their gradients. Also, if bars homogenized the SPs, we might expect a smooth transition in the line-strength profiles from the bulge to the bar. However, the outer bulges of barred galaxies have lower [MgFe]' than the inner bar, the same way the outer bulges of unbarred galaxies have lower [MgFe]' than the inner disc.

4.2.3 *Abundance ratio gradients*

Most galaxies either have a positive gradient or no gradient in Mgb/⟨Fe⟩ within the bulge-dominated region (Figs 16 and 17). The disc-dominated regions generally have solar α/Fe. Since the red-bulge galaxies have supersolar α/Fe in the centre, they have a negative gradient in the bulge–disc transition. The blue–bulge galaxies have solar α/Fe in the centre. These either have uniformly solar α/Fe or a positive gradient in the bulge and a negative gradient in the bulge-disc transition. Recall that what is marked as the bulge-dominated region in some galaxies (e.g. NGCs 266 and 5375) is actually a bar and that the true bulge-dominated region is smaller. The elliptical galaxy, NGC 4472, is uniformly supersolar in α/Fe.

There are a few galaxies that have supersolar α/Fe in the disc-dominated region. NGCs 266, 5707 and 5746 are nearly uniformly supersolar. The disc of NGC 5838 is supersolar but less enhanced than its bulge.

For NGC 3384, we obtain a positive gradient in Mgb/⟨Fe⟩ while Fisher et al. (1996; green curve in Fig. 16) found no gradient. The discrepancy could be due to scattered light in our data. The other two objects affected by scattered light are NGCs 2787 and 3945. NGC 2787 shows no gradient in Mgb/⟨Fe⟩. NGC 3945 has an asymmetric positive gradient. This could not be due entirely to scattered light since the scattered profile was symmetric.

4.3 Emission lines in bulges

Fig. 18 shows profiles of Hα and [N II] 6583 emission strength in our galaxies. We detect emission in the central regions of all our galaxies except the S0s, NGCs 3384 and 7457. The locations of our galaxies in the Baldwin et al. (1981) (hereafter BPT) diagram of emission-line ratios are shown in Fig. 19 for objects with central emission-line EW smaller than -0.5 Å (the negative sign denotes emission) in Hα, [N II] 6583, Hβ, and [O III] 5007 . The dashed curve shows the demarcation between starburst galaxies and active galactic nuclei (AGN) as defined by Kauffmann et al. (2003). The majority of our emission-line galaxies are AGN. If the emission in these galaxies is due entirely to the AGN, we would expect it to be restricted to the centre of the galaxy. However, in the three of these (NGCs 2599, 5719 and 7537), it is not centrally peaked. In the other five (NGCs 266, 2916, 3831, 5793 and 6368), the emission peaks at the centre and decreases steadily out to the edge of the bulge-dominated region, beyond which it rises again. Therefore, all

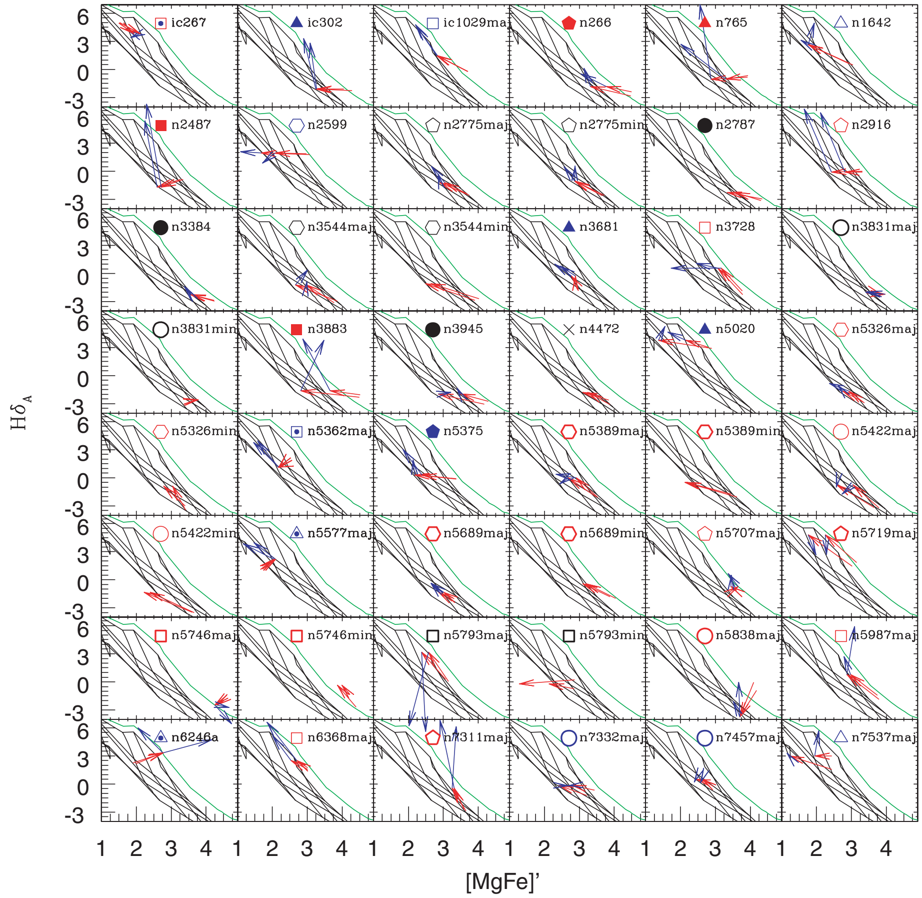

Figure 14. Gradients in Hδ_A and [MgFe]'. The red arrows are drawn from the galaxy centre to the edge of the bulge-dominated region on either side of the galaxy. The blue arrows are drawn from the edge of the bulge-dominated region to the disc scalelength. The symbols are as in Fig. 6. TMB models with solar α/Fe, age = 1, 2, 3, 6 and 15 Gyr, and [Z/H] = −1.35, −0.33, 0, 0.35 and 0.67 are overlaid. Unlike Hβ, the higher-order Balmer indices are not independent of α/Fe. α-enhanced models are parallel to the solar models, lying above and to the right-hand side. The green curves show models with age = 1 Gyr and [Z/H] =0.67 for [α/Fe] = 0.3.

or most of the AGN also have active star formation in the bulge-dominated region.

AGN have previously been found to have a larger fraction of young stars than quiescent galaxies (Raimann et al. 2001, 2003). In agreement with these results, we find that most of the AGN have small SSP ages (<4 Gyr). The only one with a large SSP age (∼15 Gyr) is NGC 3831. This could be due to errors from emission correction or from the young component not dominating the total luminosity. Prugniel et al. (2001) found that bulges with emission were small and metal poor. The star-forming region of our BPT diagram is populated by four blue bulges. They have similar SPs as Prugniel et al.'s emission-line galaxies except that one of them (NGC 6246A) has a large SSP age, again possibly due to errors in emission correction.

We see a wide range of behaviours in the emission-line profiles. In some galaxies, such as NGCs 3681 and 5362, there is strong emission in the disc-dominated region but little or no emission in the bulge-dominated region as would be expected if discs continue to form stars while bulges do not. The only galaxies with little or no emission in the disc-dominated region are S0s. In other cases, there is emission throughout the galaxy but it is weaker in the bulge-dominated region (e.g. NGCs 1642, 2916, 5020 and 7537). This is consistent with a quiescent bulge and a star-forming disc coexisting in the central regions with the ratio of bulge to disc dominance decreasing with radius. Alternatively, the bulge and disc could both be forming stars but the disc does so more actively. Finally, in some cases (e.g. IC 267 and NGCs 266 and 5793), the emission lines are strongest at the centre.

5 THE FORMATION OF BULGES

As mentioned in the Introduction section, present-day ΛCDM cosmology argues against the monolithic collapse scenario as does observational evidence for the recent and continuing mass assembly of ellipticals. Of the main proposed formation scenarios, that leaves mergers and secular evolution as possibilities for bulges.

However, the collapse model continues to receive much attention under the claim that it better reproduces the observed line-strength profiles of ellipticals. We investigate whether or not this is true for bulges. Gradients in the index Mg_2 have been computed in galaxies formed in collapse and merger simulations, allowing for direct comparisons with our data (Fig. 20). The points are our data. The solid lines are two remnants from major disc–disc mergers by Bekki & Shioya (1999) with initial disc masses of 10^{10} M$_\odot$ (bottom curve in Mg_2; top curve in Hβ) and 10^{12} M$_\odot$. The remnants are 13.1 Gyr old. The dotted lines are two collapse models by Angeletti & Giannone (2003) with final ages of 13 Gyr (top curve) and 2 Gyr. We focus on the gradient slopes, assuming that changes in mass and

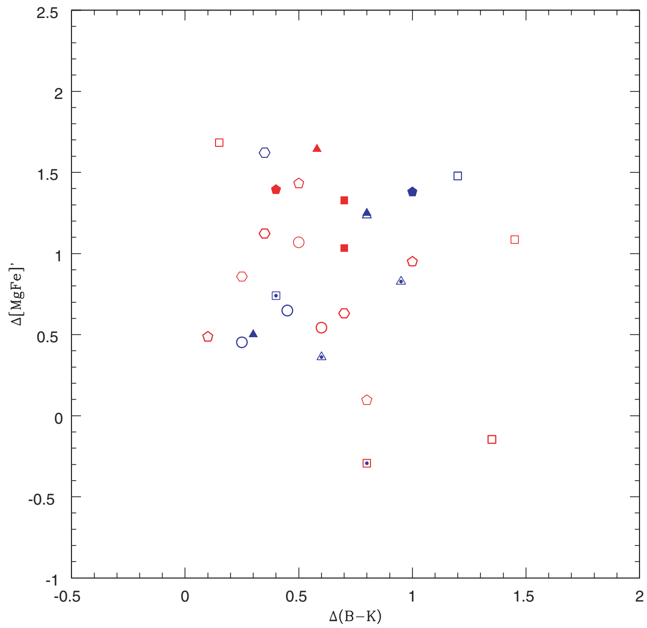

Figure 15. [MgFe]' gradient versus $B - K$ colour gradient, where a gradient is defined as the difference between the value at the centre of the galaxy and the value at the disc scalelength. The symbols are as in Fig. 6.

formation epoch mainly shift the models up or down. The collapse models predict steeper Mg_2 profiles than the merger models. Within the bulge-dominated region, some of our profiles agree with one of the merger models (e.g. NGCs 765 and 7311), while others agree with one of the collapse models (e.g. NGC 3728 and the minor-axes of NGCs 5326 and 5422). There are also cases, mostly among blue bulges, where the observed profile is flatter than the merger models (e.g. IC 302). However, the majority of galaxies fall between the collapse and merger models.

Bekki & Shioya also computed Hβ profiles in their models (Fig. 21). Nearly all our galaxies have flat Hβ profiles within the bulge-dominated region as predicted by the models. The profiles of the oldest bulges agree with the models in their zero-points as well, while younger bulges lie above the models.

Through chemical evolution modelling, Thomas et al. (1999) studied α/Fe ratios in ellipticals that formed through a fast ($\sim$1 Gyr) collapse of star-forming clumps and through mergers of MW-like spirals. The main difference between the two models was that the merging spirals had several Gyr of Fe-enrichment, while the gas involved in the collapse was not pre-enriched in Fe. The large central α/Fe ratios found in massive ellipticals were reproduced in the collapse model. The merger model does not produce supersolar α/Fe assuming a Salpeter initial mass function, unless the merger happened early, before the progenitors acquired much Fe. Metallicity and α/Fe are anticorrelated in the collapse model; since ellipticals have negative gradients in metallicity, the model predicts that they

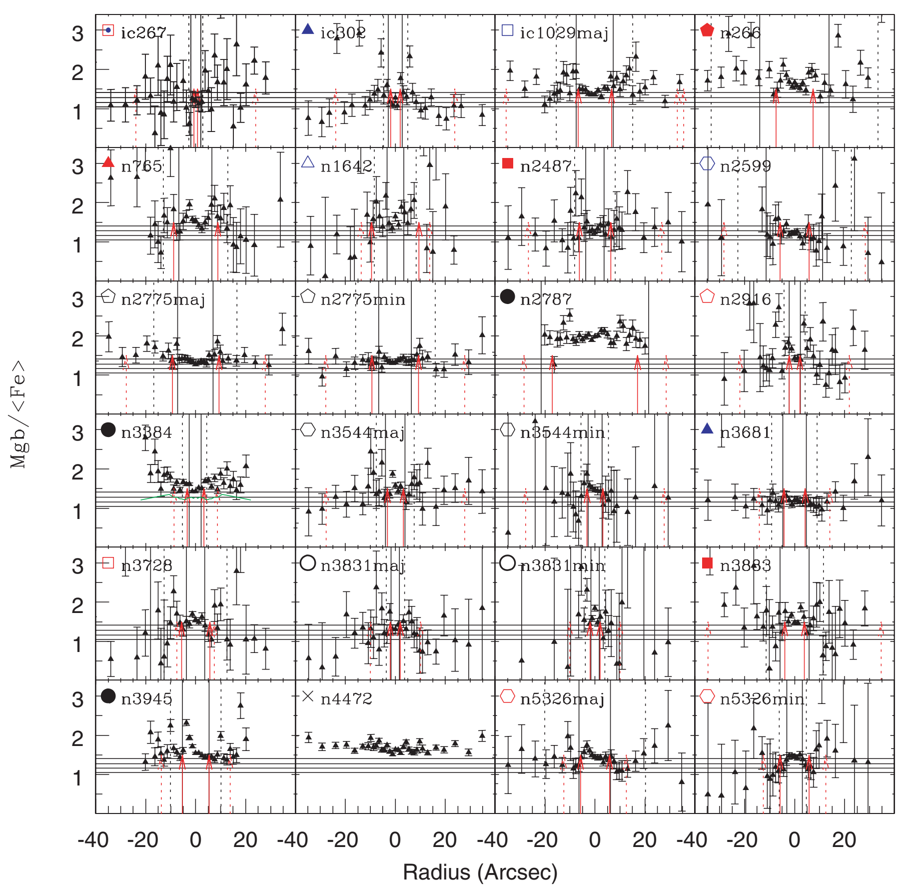

Figure 16. Mgb/⟨Fe⟩ profiles in our galaxies. For NGC 3384, the green curve shows the profile obtained by Fisher et al. (1996). The symbols are as in Fig. 6. The horizontal lines are as in Fig. 7.

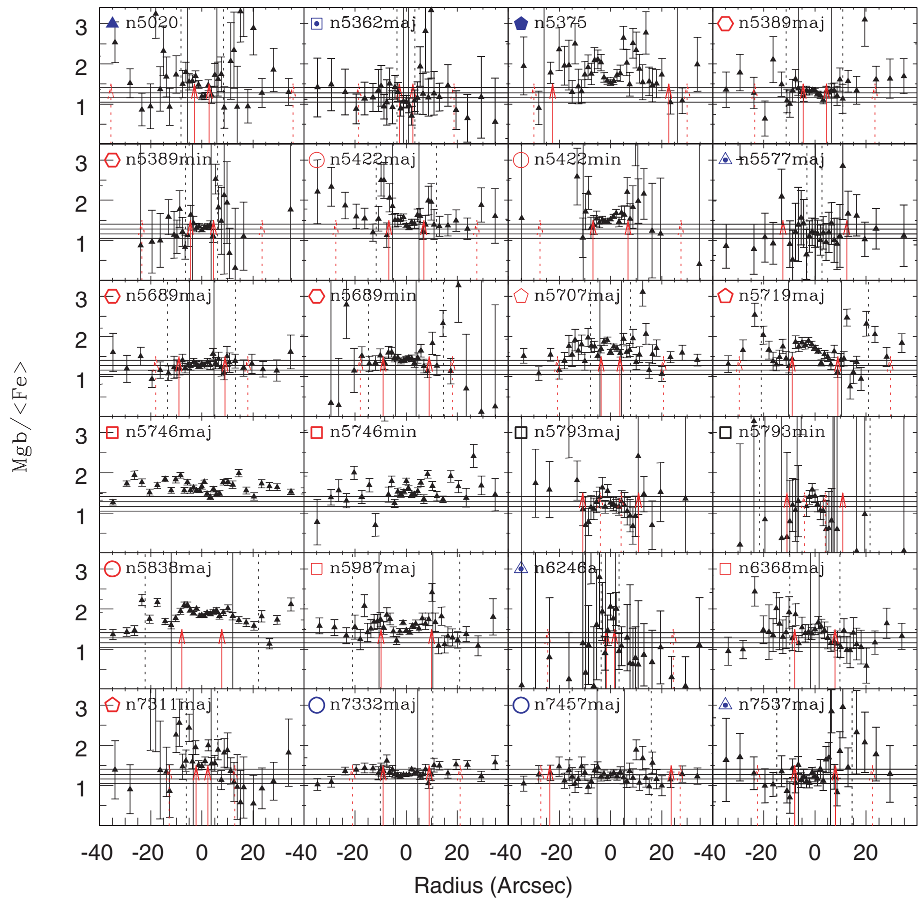

Figure 17. Mgb/⟨Fe⟩ profiles in our galaxies (continued). The symbols are as in Fig. 6. The horizontal lines are as in Fig. 7.

should have a positive gradient in α/Fe. The merger model produces solar α/Fe in the outer regions. Therefore, uniformly solar α/Fe is consistent with the merger model while positive gradients are consistent with the collapse model. Pipino et al. (2005) also found positive α/Fe gradients in a model where ellipticals are formed through the infall of gaseous lumps. Since our blue bulges have uniformly solar α/Fe, they are consistent with the predictions of the merger model. Several of the red bulges have positive gradients as predicted by the collapse model. Most of the remaining bulges have uniformly supersolar α/Fe, which is difficult to reproduce in any of the models.

In summary, both collapse and merger models have limited success in reproducing the line-strength profiles of individual galaxies but neither explain the full range of behaviours seen in the data. It is important to note that hierarchical models are only beginning to make robust predictions for SPs, successfully reproducing properties traditionally thought to favour the collapse model, such as the mass–metallicity relation. As advancements continue to be made in incorporating gas dynamics, star formation, and chemical evolution in cosmologically motivated merger models, it will be interesting to see if the line-strength profiles will be reproduced as well.

5.1 Mergers

In a recent paper, Faber et al. (2005) argued that massive red ellipticals could not have formed entirely through major mergers of gas-rich components or through dry mergers but through a combination of the two. Ellipticals of the same mass and colour could have formed in different ways: through early gas-rich mergers of low-mass objects followed by dry mergers or through recent gas-rich mergers of more-massive objects. Objects that arrived on the red sequence early-on and have been gaining mass through dry mergers will have larger SSP ages than those that have arrived on the red sequence near their present mass as the result of recent gas-rich mergers. The former will also have smaller metallicities since their last gas-rich mergers were of lower-mass progenitors with correspondingly lower metallicities according to the gas-phase mass–metallicity relation (Kobulnicky et al. 2003; Tremonti et al. 2004). The predicted anticorrelation between age and metallicity at fixed σ_0 is seen in ellipticals. If such an anticorrelation exists for bulges, it is not nearly as tight as that of ellipticals. This suggests that an additional formation mechanism might be required to explain the SPs of bulges.

Recent semi-analytic models incorporating the Millenium Simulation of cosmic structure growth find a correlation between stellar metallicity and stellar mass, with the most-massive galaxies having roughly solar metallicity (De Lucia et al. 2006). This is qualitatively consistent with the observed [MgFe]'–σ_0 and [MgFe]'–$V_{\max}$ relations. Massive ellipticals and bulges have supersolar central metallicity which is in apparent contradiction with De Lucia et al.'s results. However, they also have negative metallicity gradients. The arrows in Fig. 12, which extend to approximately the bulge effective radius, fall around solar metallicity in the massive red bulges. The metallicity at the effective radius is more representative, than the central value, of the mean metallicity. Therefore, the data are not inconsistent with the models.

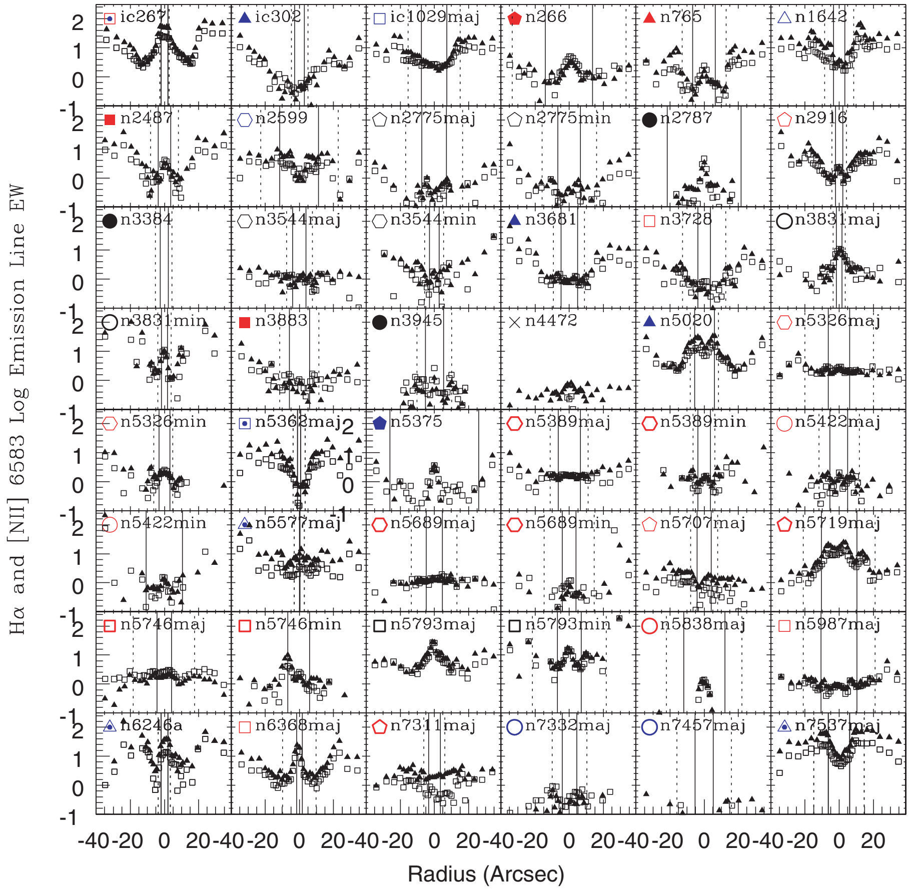

Figure 18. Profiles of emission-line strengths in bulges. The triangles are Hα. The squares are [N II] 6583. The symbols are as in Fig. 6.

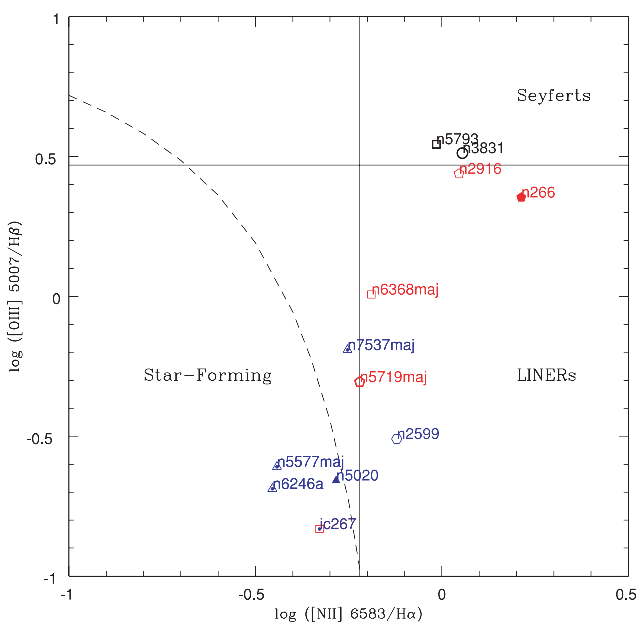

Figure 19. Bulges on the BPT (Baldwin et al. 1981) diagram in which the emission-line flux ratio [O III] 5007/Hβ is plotted against the ratio [N II] 6583/Hα. The symbols are as in Fig. 8. The dashed curve shows the demarcation between starburst galaxies and AGN as defined by Kauffmann et al. (2003). We adopt the commonly used definition of LINERs having [O III] 5007/Hβ $<$ 3 and [N II] 6583/Hα $>$ 0.6 and Seyferts having [O III] 5007/Hβ $>$ 3 and [N II] 6583/Hα $>$ 0.6.

De Lucia et al. also found in their simulations that less-massive ellipticals had more extended star formation histories than their massive counterparts. This is consistent with the observed α/Fe–σ_0 and α/Fe–$V_{\rm max}$ correlations. These correlations can be produced in starbursts induced by gas-rich mergers. During the starburst, SNe II enrich the ISM with α-elements. If star formation is somehow quenched before SNe Ia contribute much Fe, the α/Fe ratio increases. Subsequent dry mergers might add scatter to the α/Fe–$V_{\rm max}$ relations by increasing $V_{\rm max}$ without altering α/Fe. The effect of dry mergers on the α/Fe–σ_0 relation is less certain. Simulations find that dry mergers increase the velocity dispersion but that the increase is more dramatic in the outer regions than at the centre (Colín et al. 2004).

The differences between blue and red bulges at fixed σ_0 can also be explained by mergers. At fixed σ_0, blue bulges have smaller SSP ages than their red counterparts which suggests that they have undergone gas-rich mergers more recently. The progenitors of the blue bulges have then had more time to acquire Fe. Since the progenitors have small α/Fe ratios, so do the remnants. This is seen in the simulations by Thomas et al. (1999), who found that gas-rich mergers cannot produce large α/Fe ratios, unless they happened early in the chemical evolution of the progenitors.

5.2 Secular evolution

In dissipationless secular evolution, the bulge is formed through the vertical and radial redistributions of disc stars. In this process, existing gradients can either become amplified since the resulting (pseudo)bulge has a smaller scalelength than the progenitor disc or

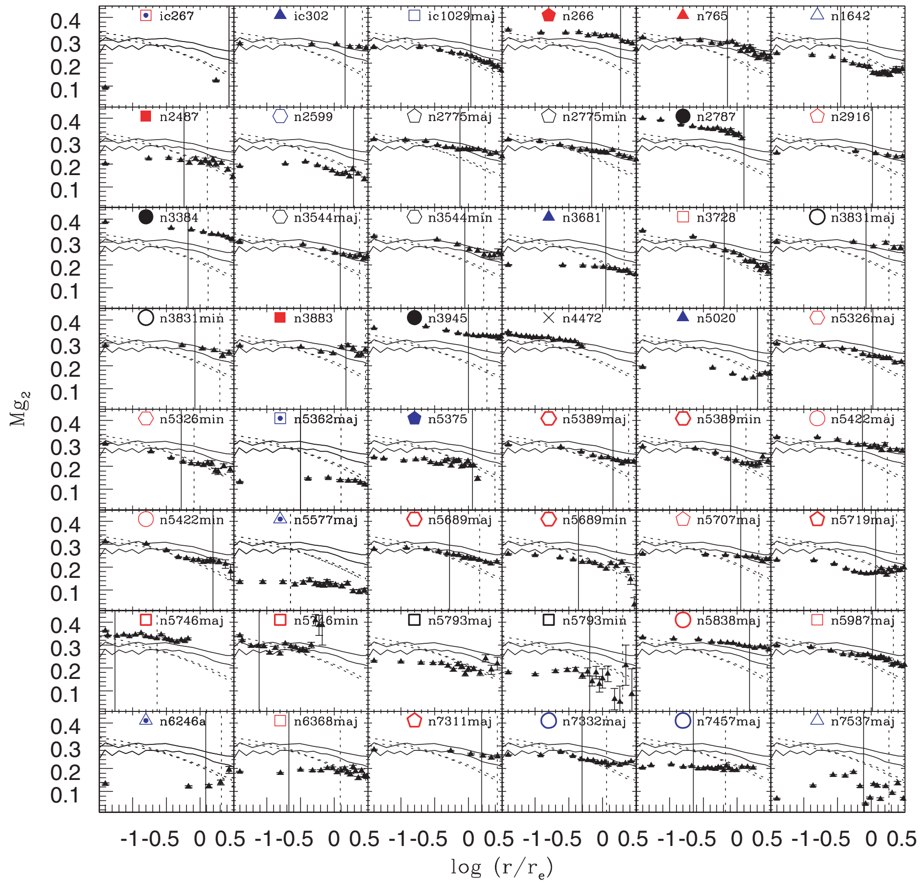

Figure 20. Comparison of Mg_2 profiles between this work and numerical simulations. The solid lines are merger models by Bekki & Shioya (1999) with final age 13.1 Gyr and initial disc masses of 10^{10} $M_{\odot}$ (bottom curve) and 10^{12} $M_{\odot}$. The dotted lines are collapse models by Angeletti & Giannone with final age 13 Gyr (top curve) and 2 Gyr. The symbols are as in Fig. 6.

erased as a consequence of disc heating. However, if the disc has no gradient, then the bulge also should not have one. This process cannot be ruled out based on [MgFe]' gradients, since the majority of galaxies show negative gradients in the disc-dominated region. However, the majority of red bulges have solar α/Fe in the disc-dominated region, despite having supersolar α/Fe in the bulge. Therefore, they could not have been produced through purely dissipationless secular evolution. If secular evolution with gas infall has been responsible for the formation of these objects, the star formation time-scales must have been identical (at fixed σ_0) in this scenario as in merger-induced star formation since red bulges and ellipticals follow the same α/Fe–σ_0 relation. Furthermore, the star formation must have been completed several Gyr ago since red bulges have large SSP ages. This goes for the three barred S0s with disc-like structural and kinematical properties (NGCs 2787, 3384 and 3945) as well. These objects are identical to ellipticals of comparable σ_0 in their SPs and two of them have among the largest central SSP ages observed.

Note that the α/Fe ratios of the blue bulges are consistent with dissipationless secular evolution. Unfortunately, neither mergers nor secular evolution can be ruled out for blue bulges based on their α/Fe ratios.

Secular evolution with gas infall is supported by the frequency of barred galaxies with age gradients. Of the 10 galaxies whose central regions are younger than the outer regions, seven are barred and one have a b/p bulge. Bar-driven gas infall could lead to extended star formation in the central region, producing the observed age gradient.

If bars are long lived and the chemical imprints of secular evolution are different from those of mergers, we would expect the bulges of barred galaxies to have different abundance patterns than those of unbarred galaxies. We see hints of such differences in index–σ_0 and index–V_{max} relations. At fixed σ_0 and V_{max}, barred galaxies appear to have larger central metallicities.

The metallicities of bulges and their discs are correlated. This is naturally explained in processes that involve the bulge being formed from the disc. However, this correlation holds for all galaxies, not just those with bars, blue bulges, or bulges identified as having disc-like structure and kinematics. Therefore, either all bulges formed secularly and some had their bars destroyed or the other bulge/disc formation mechanisms also produce this correlation.

5.3 Evolution of galaxy populations

Small-σ bulges fall into two categories: YMR bulges with little or no star formation and MP bulges which are actively forming stars. This suggests that the MP bulges would have migrated to the YMR region by the time their star formation is quenched. Will this be the scenario for all metal-poor bulges (including that of the MW) or is the observed anticorrelation between emission strength and metallicity the result of small number statistics? Are there really no metal-poor bulges that do not have emission? Extending this type

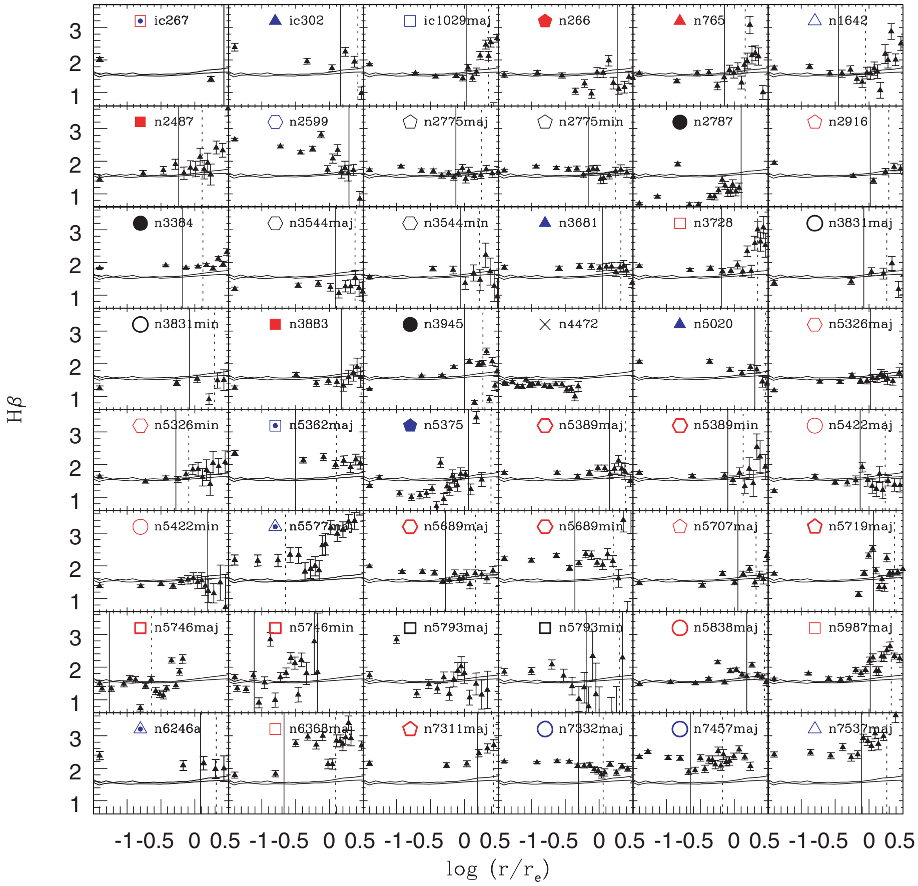

Figure 21. Comparison of Hβ profiles between this work and merger models by Bekki & Shioya (1999) with initial disc masses of 10^{10} $M_{\odot}$ (bottom curve) and 10^{12} $M_{\odot}$. The symbols are as in Fig. 6.

of study to large galaxy samples should shed light into the evolution of small-σ bulges.

While all five of the MP galaxies are late types (Sb–Sc), three of the seven YMR galaxies are early types (S0–Sa). Perhaps, the mechanisms that trigger and quench the star formation are also responsible for transforming galaxies from late to early types. As the YMR bulges age, they will move down to the OMR region.

6 SUMMARY

We have studied line strengths in the bulges and inner discs of 38 galaxies in the local Universe. Our galaxies span a wide range of Hubble types, central velocity dispersions, maximum disc rotational velocities, and inclinations. The low-inclination galaxies include barred and unbarred objects; the edge-on galaxies include those with and without b/p bulges. We included several galaxies whose bulges were previously identified as being disc like in their colours or kinematics to see if their spectral properties reveal evidence for secular evolution. We use the [MgFe]' index and five Balmer indices to characterize the luminosity-weighted metallicities and ages of the SPs and the Mgb/⟨Fe⟩ index to characterize the α/Fe ratios. Our main results are the following.

(i) The central regions of bulges range in SSP metallicity from [Z/H] = −0.8 to +0.7 dex and in SSP age from less than 2 to greater than 15 Gyr.

(ii) The central ages and metallicities are sensitive to bulge colour which is in turn sensitive to central velocity dispersion and maximum disc rotational velocity.

(iii) Red bulges of all Hubble types are similar to luminous ellipticals in their central SPs. They have large SSP ages and are supersolar in SSP metallicity and α/Fe.

(iv) Blue bulges can be separated into two classes: a metal-poor class that is restricted to late types with small velocity dispersion and a young, metal-rich class that includes all Hubble types and velocity dispersions. The metal-poor blue bulges are actively forming stars, while the metal-rich ones are not. Low-luminosity ellipticals exhibit a similar range of SSP ages and metallicities as blue bulges.

(v) Luminous ellipticals and the different types of bulges form a continuous and overlapping sequence on diagrams of metallicity- and age-sensitive indices versus σ_0. At fixed σ_0, there is no systematic difference between bulges and ellipticals on these diagrams but bulges exhibit larger scatter. At fixed σ_0, age and metallicity are more tightly anticorrelated in ellipticals than in bulges.

(vi) α/Fe in red bulges is correlated with σ_0 and V_{max}. Red bulges and ellipticals follow the same α/Fe–σ_0 relation.

(vii) Most blue bulges (11 out of 14) are consistent with having solar α/Fe. At fixed σ_0, blue bulges have smaller α/Fe than red bulges and ellipticals.

(viii) Barred galaxies appear to have larger central metallicities than unbarred galaxies of the same σ_0 and V_{max}.

(ix) Most galaxies show a steady decrease in metallicity-sensitive indices with radius. The slope of the gradient is correlated with the central value and therefore with the global kinematics. The bulge- and disc-dominated regions are distinct in their line-strength profiles, with the discs generally having shallower slopes. The smallest bulges do not have negative line-strength gradients; some of these have flat profiles in the central region while others have positive gradients.

(x) There is a correlation between [MgFe]' strength in the bulge and the disc. This correlation holds for all galaxies, not just those with bars, blue bulges, or bulges identified as having disc-like structural or kinematical properties.

(xi) Where positive age gradients (with the central regions being younger) are present, they are invariably in barred galaxies. This suggests that bar-driven star formation has occurred. However, several red bulges in barred galaxies have large central SSP ages (although it could be younger than those in the outer regions) which means there has been no significant bar-driven star formation for several Gyr.

(xii) Four galaxies have supersolar α/Fe in the disc-dominated region. The rest are consistent with having solar α/Fe in the disc.

(xiii) Objects identified as having disc-like structural or kinematical properties do not have notably different SPs than other bulges. They follow the same scaling relations as the red bulges and ellipticals and have metallicity gradients. The three barred S0s identified as having bulges with disc-like structural and kinematical properties are also α-enhanced and therefore do not resemble the majority of the discs, including the MW disc at the solar neighbourhood.

(xiv) Colour profiles agree frequently but not always with line-strength profiles. Where discrepancies exist, they are likely due to differences in age- and metallicity-sensitivity between colours and line strengths and to the colours being affected by dust. Consequently, colour gradients do not necessarily correlate with [MgFe]' gradients.

Overall, our results are consistent with the hypothesis that mergers have been the dominant mechanism responsible for the formation of bulges. However, some of the observations, such as the correlation between bulge and disc metallicity, pose significant challenges to the merger scenario. Furthermore, the possibility that barred galaxies follow different scaling relations than unbarred galaxies and are overrepresented among galaxies with age gradients supports the secular evolution picture.

Central line strengths on a statistically significant sample of ellipticals and bulges of barred and unbarred spirals would be invaluable in determining whether more than one formation mechanism is required for bulges. The necessary data are already available in the data bases of large surveys such as the Sloan Digital Sky Survey (SDSS). Spatially resolved studies on a smaller, representative sample, would allow for better comparisons between gradients in different types of galaxies.

ACKNOWLEDGMENTS

It is a pleasure to thank Anatoly Klypin, Jason Peterson, Jesús Falcón-Barroso, Mike Hudson, Jenica Nelan, Reynier Peletier, Claudia Maraston, Daniel Thomas, Scott Trager, and Guy Worthey for helpful discussions or assistance with the data analysis. We would also like to thank the anonymous referee for suggestions that greatly improved this manuscript. Partial funding was provided by the New Mexico Space Grant Consortium. This research has made use of the NASA/IPAC Extragalactic Data base (NED) which is operated by the Jet Propulsion Laboratory, California Institute of Technology, under contract with the National Aeronautics and Space Administration.

REFERENCES

Abadi M. G., Navarro J. F., Steinmetz M., Eke V. R., 2003, ApJ, 597, 21
Andredakis Y. C., Sanders R. H., 1994, MNRAS, 267, 283
Angeletti L., Giannone P., 2003, A&A, 403, 449
Arimoto N., Yoshii Y., 1987, A&A, 173, 23
Aronica G., Athanassoula E., Bureau M., Bosma A., Dettmar R.-J., Vergani D., Pohlen M., 2003, AP&SS, 284, 753
Athanassoula E., 2005, MNRAS, 358, 1477
Athanassoula E., Misiriotis A., 2002, MNRAS, 330, 35
Balcells M., Peletier R. F., 1994, AJ, 107, 135
Balcells M., Graham A. W., Domínguez-Palmero L., Peletier R. F., 2003, ApJ, 582, L79
Baldwin J. A., Phillips M. M., Terlevich R., 1981, PASP, 93, 5 (BPT)
Bekki K., Shioya Y., 1999, ApJ, 513, 108
Bell E. F. et al., 2004, ApJ, 608, 752
Bender R., Burstein D., Faber S. M., 1993, ApJ, 411, 153
Bertola F., Capaccioli M., 1977, ApJ, 211, 697
Bournaud F., Combes F., Semelin B., 2005, MNRAS, pp L89+
Bruzual G., Charlot S., 2003, MNRAS, 344, 1000 (BC03)
Bureau M., Freeman K. C., 1999, AJ, 118, 126
Burstein D., Faber S. M., Gaskell C. M., Krumm N., 1984, ApJ, 287, 586
Busarello G., Capaccioli M., D'Onofrio M., Longo G., Richter G., Zaggia S., 1996, A&A, 314, 32
Caldwell N., Rose J. A., Concannon K. D., 2003, AJ, 125, 2891
Cappellari M., Emsellem E., 2004, PASP, 116, 138
Carlberg R. G., 1984, ApJ, 286, 403
Carollo C. M., Danziger I. J., Buson L., 1993, MNRAS, 265, 553
Carollo C. M., Stiavelli M., de Zeeuw P. T., Mack J., 1997, AJ, 114, 2366
Chung A., Bureau M., 2004, AJ, 127, 3192
Colín P., Klypin A., Valenzuela O., Gottlöber S., 2004, ApJ, 612, 50
Combes F., Debbasch F., Friedli D., Pfenniger D., 1990, A&A, 233, 82
Courteau S., de Jong R. S., Broeils A. H., 1996, ApJ, 457, L73
Davidge T. J., 2001, AJ, 122, 1386
de Jong R. S., 1996a, A&AS, 118, 557
de Jong R. S., 1996b, A&A, 313, 377 (DJ)
de Jong R. S., Simard L., Davies R. L., Saglia R. P., Burstein D., Colless M., McMahan R., Wegner G., 2004, MNRAS, 355, 1155
De Lucia G., Springel V., White S. D. M., Croton D., Kauffmann G., 2006, MNRAS, 366, 499
de Vaucouleurs G., de Vaucouleurs A., Corwin H. G., Buta R. J., Paturel G., Fouque P., 1991, Third Reference Catalogue of Bright Galaxies, Vols 1–3. Springer-Verlag, Berlin, Heidelberg, New York, p. 7
de Zeeuw P. T. et al., 2002, MNRAS, 329, 513
Debattista V. P., Carollo C. M., Mayer L., Moore B., 2004, ApJ, 604, L93
Denicoló G., Terlevich R., Terlevich E., Forbes D. A., Terlevich A., 2005, MNRAS, 358, 813
Emsellem E. et al., 2004, MNRAS, 352, 721
Erwin P., Beltrán J. C. V., Graham A. W., Beckman J. E., 2003, ApJ, 597, 929
Faber S. M., Friel E. D., Burstein D., Gaskell C. M., 1985, ApJS, 57, 711
Faber S. M. et al., 2005, ApJ, submitted (astro-ph/0506044)
Fairall A. P. et al., 1992, AJ, 103, 11
Falcón-Barroso J., Peletier R. F., Balcells M., 2002, MNRAS, 335, 741
Falcón-Barroso J. et al., 2004, MNRAS, 350, 35
Feltzing S., Gilmore G., 2000, A&A, 355, 949
Ferreiro D. L., Pastoriza M. G., 2004, A&A, 428, 837
Fisher D., Franx M., Illingworth G., 1996, ApJ, 459, 110
Forbes D. A., Sánchez-Blázquez P., Proctor R., 2005, MNRAS, 361, L47
Friedli D., Benz W., 1995, A&A, 301, 649
Friedli D., Benz W., Kennicutt R., 1994, ApJ, 430, L105
Fulbright J. P., McWilliam A., Rich R. M., 2006, ApJ, 636, 821
Gadotti D. A., dos Anjos S., 2001, AJ, 122, 1298
Goudfrooij P., Gorgas J., Jablonka P., 1999, AP&SS, 269, 109
Ibata R. A., Gilmore G. F., 1995, MNRAS, 275, 605
Idiart T. P., de Freitas Pacheco J. A., Costa R. D. D., 1996, AJ, 112, 2541
Immeli A., Samland M., Gerhard O., Westera P., 2004, A&A, 413, 547

Jablonka P., Martin P., Arimoto N., 1996, AJ, 112, 1415
Jablonka P., Courbin F., Meylan G., Sarajedini A., Bridges T. J., Magain P., 2000, A&A, 359, 131
Jablonka P., Gorgas J., Goudfrooij P., 2002, AP&SS, 281, 367
Kannappan S. J., Jansen R. A., Barton E. J., 2004, AJ, 127, 1371
Karachentsev I. D., Makarov D. A., 1996, AJ, 111, 794
Kauffmann G., 1996, MNRAS, 281, 487
Kauffmann G., White S. D. M., Guiderdoni B., 1993, MNRAS, 264, 201
Kauffmann G. et al., 2003, MNRAS, 346, 1055
Kobayashi C., Arimoto N., 1999, ApJ, 527, 573
Kobulnicky H. A. et al., 2003, ApJ, 599, 1006
Kormendy J., 1993, in Dejonghe H., Habing H. J., eds, IAU Symp. 153, Galactic Bulges. Kluwer, Dordrecht, p. 209
Kormendy J., Illingworth G., 1982, ApJ, 256, 460
Kormendy J., Kennicutt R. C., 2004, ARA&A, 42, 603
Kuntschner H. et al., 2006, MNRAS, 369, 497
Lütticke R., Dettmar R.-J., Pohlen M., 2000, A&AS, 145, 405
Larson R. B., 1974, MNRAS, 166, 585
Lee H.-c., Worthey G., 2005, ApJS, 160, 176
MacArthur L. A., 2005, ApJ, 623, 795
MacArthur L. A., Courteau S., Holtzman J. A., 2003, ApJ, 582, 689
Massey P., Strobel K., Barnes J. V., Anderson E., 1988, ApJ, 328, 315
Mehlert D., Thomas D., Saglia R. P., Bender R., Wegner G., 2003, A&A, 407, 423
Michard R., Marchal J., 1994, A&AS, 107, 187
Minniti D., 1996, ApJ, 459, 175
Nelan J. E., Smith R. J., Hudson M. J., Wegner G. A., Lucey J. R., Moore S. A. W., Quinney S. J., Suntzeff N. B., 2005, ApJ, 632, 137
Nilson P., 1973, Uppsala general catalogue of galaxies. Acta Universitatis Upsaliensis. Nova Acta Regiae Societatis Scientiarum, Series V
Noguchi M., 2000, MNRAS, 312, 194
Norman C. A., Sellwood J. A., Hasan H., 1996, ApJ, 462, 114
Peletier R. F., Balcells M., 1997, New Astron., 1, 349 (PB)
Peletier R. F., Vazdekis A., Arribas S., del Burgo C., García-Lorenzo B., Gutiérrez C., Mediavilla E., Prada F., 1999, MNRAS, 310, 863
Pfenniger D., 1993, in Dejonghe H., Habing H. J., eds, IAU Symp. 153, Galactic Bulges. Kluwer, Dordrecht, p. 387
Pipino A., Kawata D., Gibson B. K., Matteucci F., 2005, A&A, 434, 553
Pinkney J. et al., 2003, ApJ, 596, 903
Proctor R. N., Sansom A. E., 2002, MNRAS, 333, 517
Proctor R. N., Sansom A. E., Reid I. N., 2000, MNRAS, 311, 37
Prugniel P., Maubon G., Simien F., 2001, A&A, 366, 68
Puzia T. H., Saglia R. P., Kissler-Patig M., Maraston C., Greggio L., Renzini A., Ortolani S., 2002, A&A, 395, 45
Puzia T. H., Perrett K. M., Bridges T. J., 2005, A&A, 434, 909
Raimann D., Storchi-Bergmann T., Bica E., Alloin D., 2001, MNRAS, 324, 1087
Raimann D., Storchi-Bergmann T., González Delgado R. M., Cid Fernandes R., Heckman T., Leitherer C., Schmitt H., 2003, MNRAS, 339, 772
Rich R. M., 1999, in Hubeny I., Heap S., Cornett R., eds, ASP Conf. Ser., Vol. 192, Spectrophotometric Dating of Stars and Galaxies. Astron. Soc. Pac., San Francisco, p. 215
Rose J. A., Bower R. G., Caldwell N., Ellis R. S., Sharples R. M., Teague P., 1994, AJ, 108, 2054
Ryder S. D., Fenner Y., Gibson B. K., 2005, MNRAS, 358, 1337
Sadler E. M., Rich R. M., Terndrup D. M., 1996, AJ, 112, 171
Sarajedini A., Jablonka P., 2005, AJ, 130, 1627
Sellwood J. A., 1993, in Dejonghe H., Habing H. J., eds, IAU Symp. 153, Galactic Bulges. Kluwer, Dordrecht, p. 391
Shen J., Sellwood J. A., 2004, ApJ, 604, 614
Sil'chenko O. K., 1999, AJ, 117, 2725
Sil'chenko O. K., Afanasiev V. L., Chavushyan V. H., Valdes J. R., 2002, ApJ, 577, 668
Sil'chenko O. K., Moiseev A. V., Afanasiev V. L., Chavushyan V. H., Valdes J. R., 2003, ApJ, 591, 185
Stephens A. W. et al., 2003, AJ, 125, 2473
Tanvir N. R., Ferguson H. C., Shanks T., 1999, MNRAS, 310, 175
Thomas D., 1999, MNRAS, 306, 655
Thomas D., Maraston C., Bender R., 2003, MNRAS, 339, 897 (TMB)
Thomas D., Maraston C., Korn A., 2004, MNRAS, 351, L19
Thomas D., Maraston C., Bender R., de Oliveira C. M., 2005, ApJ, 621, 673
Trager S. C., Worthey G., Faber S. M., Burstein D., Gonzalez J. J., 1998, ApJS, 116, 1
Trager S. C., Faber S. M., Worthey G., González J. J., 2000a, AJ, 119, 1645
Trager S. C., Faber S. M., Worthey G., González J. J., 2000b, AJ, 120, 165
Tremonti C. A. et al., 2004, ApJ, 613, 898
Tripicco M. J., Bell R. A., 1995, AJ, 110, 3035
van Dokkum P. G., 2005, AJ, 130, 2647
van Dokkum P. G., Franx M., Fabricant D., Kelson D. D., Illingworth G. D., 1999, ApJ, 520, L95
van Loon J. T. et al., 2003, MNRAS, 338, 857
Vazdekis A., 1999, ApJ, 513, 224
Vazdekis A., Peletier R. F., Beckman J. E., Casuso E., 1997, ApJS, 111, 203
Vazdekis A., Kuntschner H., Davies R. L., Arimoto N., Nakamura O., Peletier R., 2001, ApJ, 551, L127
Wegner G., da Costa L. N., Alonso M. V., Bernardi M., Wilmer C. N. A., Pellegrini P. S., Rité C., Maia M., 2000, in Courteau S., Willick J., eds, ASP Conf. Ser., Vol. 201, Cosmic Flows Workshop. Astron. Soc. Pac., San Francisco, p. 62
White S. D. M., 1980, MNRAS, 191, 1P
Worthey G., 1994, ApJS, 95, 107
Worthey G., Ottaviani D. L., 1997, ApJS, 111, 377
Worthey G., Collobert M., 2003, ApJ, 586, 17
Worthey G., Faber S. M., Gonzalez J. J., Burstein D., 1994, ApJS, 94, 687
Wyse R. F. G., Gilmore G., Franx M., 1997, ARA&A, 35, 637
Zoccali M. et al., 2003, A&A, 399, 931

This paper has been typeset from a TEX/LATEX file prepared by the author.